

This manuscript is a preprint and has been submitted for publication in **Basin Research**. Please note that this manuscript has not yet undergone peer-review; as such, subsequent version of this manuscript may have different content. We invite you to contact any of the authors directly to comment and give any feedbacks on the manuscripts.

Pre-salt rift morphology controls salt tectonics in the Campos Basin, offshore SE Brazil

Francyne Bochi do Amarante^{1,2,#}

¹ Instituto de Geociências, Universidade Federal do Rio Grande do Sul, Porto Alegre, 90650 001, Brazil

² Basins Research Group (BRG), Department of Earth Science and Engineering, Imperial College London, London, SW7 2BP, United Kingdom

corresponding author francyne.amarante@ufrgs.br

ORCID <https://orcid.org/0000-0003-4452-8635>

Christopher Aiden-Lee Jackson²

² Basins Research Group (BRG), Department of Earth Science and Engineering, Imperial College London, London, SW7 2BP, United Kingdom

c.jackson@imperial.ac.uk

ORCID <https://orcid.org/0000-0002-8592-9032>

Leonardo Muniz Pichel^{2,3}

² Basins Research Group (BRG), Department of Earth Science and Engineering, Imperial College London, London, SW7 2BP, United Kingdom

³ Department of Earth Science, University of Bergen, Allegaten 41, 5007, Bergen, Norway

l.muniz-pereira@imperial.ac.uk

ORCID <https://orcid.org/0000-0001-8692-3831>

Claiton Marlon dos Santos Scherer¹

¹ Instituto de Geociências, Universidade Federal do Rio Grande do Sul, Porto Alegre, 90650 001, Brazil

claiton.scherer@ufrgs.br

ORCID <https://orcid.org/0000-0002-7520-1187>

Juliano Kuchle¹

¹ Instituto de Geociências, Universidade Federal do Rio Grande do Sul, Porto Alegre, 90650 001, Brazil

juliano.kuchle@ufrgs.br

ORCID <https://orcid.org/0000-0003-4325-0547>

Funding statement/information

Sandwich Doctorate Abroad Scholarship (SWE) from CNPq (Brazilian Council for Scientific and Technological Development). Grant/Award number: 202497/2019-4.

Data Availability Statement

The seismic and well data supporting this study were made available by ANP (Brazilian Agency of Petroleum, Natural Gas and Biofuels). The authors are not allowed to share the data, which were used under license for this study.

The authors declare no conflict of interest.

Abstract

Classic models of gravity-driven salt tectonics commonly depict kinematically linked zones of overburden deformation, characterised by updip extension and downdip contraction, separated by a weakly deformed zone associated with downdip translation above a relatively smooth base-salt surface. We use 2D and 3D seismic reflection and borehole data from the south-central Campos Basin to show that these models fail to adequately capture the complex range of structural styles forming during salt-detached gravity-driven deformation above a rugose base-salt surface. In the Campos Basin the base-salt is defined by broadly NE-trending, margin-parallel, generally seaward-dipping ramps with up to 2 km of structural relief. We define three domains of overburden deformation: an updip extensional domain, an intermediate multiphase domain, and a downdip contractional domain. The multiphase domain is defined by large, partly fault-bounded, ramp-syncline basins, the stratigraphic record of which suggest c. 35 km of seaward (horizontal) gravity-driven translation of salt and its overburden since the Albian. We also identify three main types of salt structures in the multiphase domain: (i) contractional anticlines that were subjected to later extension and normal faulting; (ii) passive-to-active diapirs that were later extended and widened, and which are bound on their landward margins by landward-dipping, salt-detached normal faults; and (iii) reactive (extensional) diapirs that was subsequently squeezed. We argue that this multiphase, hybrid-style of deformation occurs as a consequence of basinward translation of salt and its overburden over complex base-salt relief, consistent with the predictions of physical models and several other 3D seismic reflection data-based studies. Critically, these local strains overprint margin-scale patterns of deformation producing kinematically-variable and multiphase salt-related deformation.

Keywords: base-salt relief, rift basin, passive margin, South Atlantic basins, ramp syncline basins, gravity-driven deformation, salt translation.

1 - Introduction

Salt-bearing passive margins typically deform in response to processes known as gravity gliding and gravity spreading (Peel, 2014). Such margins can be divided into kinematically linked domains of deformation, each associated with a distinct suite of salt and overburden structures (e.g. Rowan et al., 2004; Brun and Fort, 2011; Peel, 2014). The upslope domain is characterised by thin-skinned (i.e. salt-detached) extension, which is associated with the formation of listric normal faults, rafts, and salt rollers (e.g. Lundin, 1992; Brun and Mauduit, 2009; Jackson and Hudec, 2017). Updip extension is accommodated by downdip contraction and the formation of salt-cored anticlines and salt-detached thrusts (e.g. Demercian et al., 1993; Brun and Fort, 2004; Fort et al., 2004). Domains of extension and contraction are separated by a domain of translation, in which deformation is typically described as being relatively mild (Brun and Fort, 2004; Davison et al., 2012).

Recent studies on South Atlantic salt basins have demonstrated that this structural zonation is an oversimplification. More specifically, these studies show that various extensional and contractional structures, in addition to ramp-syncline basins (RSBs), can form in the translational domain due to the flow of salt and overburden across base-salt relief associated with prior rifting (Brun and Fort 2004, 2011; Dooley et al., 2017; Hudec et al., 2013; Pichel et al., 2018, 2019a; Evans and Jackson, 2020; Erdi and Jackson, 2021). Local deformation can overprint regional patterns of deformation, resulting in multiphase structures with a complex kinematic history (Dooley et al., 2017; Pichel et al., 2019b; Erdi and Jackson, 2021).

The Aptian salt basin offshore southeastern Brazil contains substantial volumes of hydrocarbons and, because of this, has been intensively studied by the energy industry since the 1970's (Mohriak et al., 1990). The Campos Basin has complex and prolific petroleum systems, and there are presently 62 producing oilfields – mainly oil, gas secondarily (ANP, 2020). These oilfields include at least four petroleum systems, with reservoirs in rift and Aptian

pre-salt clastics and carbonates, Albian/Cenomanian marine carbonates, and most importantly Upper Cretaceous to Eocene clastic turbidites (Guardado et al., 1989; Bruhn et al., 2003). The salt and its tectonics have main role on oil accumulation, composing different elements in all known petroleum systems (Guardado et al., 1989; Mohriak et al., 2012). Salt can be the seal rock, mainly to rift and Aptian pre-salt accumulations; salt structures (more specifically thin-skinned faulting above salt anticlines and rollers) can compose traps to post-salt turbidites; the absence of salt can delineate pathways hydrocarbon migration, and salt driven faults can act as both migration pathways and traps depending on their location and stratigraphic level. Despite its importance, there are surprisingly few publications on the salt tectonics of the Campos Basin (Cobbold and Szatmari, 1991; Demercian et al., 1993; Rouby et al., 1993; Mohriak et al., 2008 Davison et al., 2012; Quirk et al., 2012), and only a few present a detailed, regional-scale analysis of the geometry and kinematics of the salt and overburden structures (Demercian et al., 1993; Rouby et al., 1993). An improved knowledge of salt tectonics is required to understand the timing of salt-related deformation and to push the hydrocarbon exploration barriers further basinward into deeper waters.

In the present study, we use 2D and 3D seismic reflection and borehole data to characterise the salt-tectonic structural styles and related evolution of salt and overburden structures in the south-central Campos Basin, SE Brazil. We first describe the extensional and contractional domains, before focusing on the boundary between the two, which we herein name the *multiphase domain*. We then investigate the evolution of extensional and contractional deformation through time and space. The discussion encompasses the effects of base-salt relief on the distribution, origin and evolution of salt and overburden structures, and the implications of our work for post-salt hydrocarbon exploration in the deep-water Campos Basin.

2 - Geological Context

The Campos Basin (c. 100,000 km²) is located on the southeastern Brazilian margin, offshore the states of Rio de Janeiro and Espírito Santo (Figure 1a) (Winter et al., 2007). The basin originated during rifting of the Gondwana Supercontinent that culminated in the opening of the South Atlantic Ocean in the Late Jurassic-to-Early Cretaceous (Figure 1b) (Szatmari, 2000). The basin is limited to the north by the Vitória High, to the south by the Cabo Frio High (Figure 2a), to the east by oceanic crust, and to the west by exposures of crystalline basement rocks of the Ribeira Belt (Mohriak et al., 1989).

The syn-rift stage of the Campos Basin (Hauterivian – Early Aptian) (Figure 1b) initiated with intense volcanic activity, contemporary to the Serra Geral volcanism documented in the Paraná Basin (Mizusaki et al., 1998). Rifting was associated with the formation of NE-SW-striking normal faults that bound horsts and grabens (Figure 2a) (Chang et al., 1992; Guardado et al., 2000). The inner (i.e. marginal) hinge line of the rift system is delineated by the Campos Fault (Figure 2a), a large structure that separates the shallow, western part, where Tertiary deposits rest directly on basement, from the deeper, eastern portion, where thick, Barremian to Aptian sediment accumulations fill rift-related depocentres (Figure 2c) (Guardado et al., 1989).

The early post-rift (i.e. sag) stage commenced in the Aptian (Figure 1b), marking the transition from basement-involved faulting and relatively rapid subsidence, to a period defined by very little faulting and long-wavelength, relatively low subsidence driven by post-rift cooling of the lithosphere. Because of this change in subsidence pattern and rate, the depositional area enlarged and sedimentation progressively draped and essentially ‘healed’ rift-related relief (Quirk et al., 2013; Kukla et al., 2018; Amarante et al., 2020). During the late Aptian, a thick salt layer was deposited in response to episodic marine-water influx through the Walvis Ridge volcanic high to the south (Davison et al., 2012). Even though salt deposition

occurred late in the sag phase, relief inherited from the rift phase still locally influenced salt distribution (Dooley et al., 2017; Davison et al., 2012).

The end of evaporitic deposition is marked by a rapid marine transgression linked to the initiation of the drift (i.e. late post-rift) stage (Albian – Present) (Figure 1b) (Chang et al., 1992). Focusing of thermally induced subsidence near the location of continental breakup caused the basin to tilt southeastward, inducing gravity gliding of Aptian salt and its overburden (Quirk et al., 2012). Major progradation of basin-margin clastic wedges commenced in the Eocene and continues to the present day (Contreras et al., 2010).

Salt-related deformation in the central South Atlantic region began in the Aptian during salt deposition (Figure 1b) (Cobbold and Szatmari, 1991; Fiduk and Rowan, 2012; Davison et al., 2012). Significant seaward flow of salt translation of its overburden is thought to have begun in the Albian and ended in the Maastrichtian (Figure 1b) (Quirk et al., 2012). Based on salt (and overburden) structural style, the Campos Basin is divided into a proximal extensional domain (70 - 200 km wide) and a distal contractional domain (70 - 300 km wide), the latter terminating seaward in a broad (up to 37 km wide) allochthonous salt sheet emplaced on the outer basement high (Figures 2b and 2c) (Davison, 2007; Davison et al., 2012). Previous works identify rafts, salt rollers, extensional anticlines, triangular-shaped salt walls, and collapsed diapirs in the extensional domain, with all these structures related, in some way, to landward- and seaward-dipping, salt-detached normal faults (Demercian et al., 1993; Mohriak et al., 2008; Quirk et al., 2012). Further seaward in the translation domain, Dooley et al. (2017) describe a ramp syncline basin. The contractional domain is characterized by elongate salt walls (Demercian et al., 1993) and polyharmonic, salt-detached (buckle) fold belts (Cobbold and Szatmari, 1991; Dooley et al., 2017).

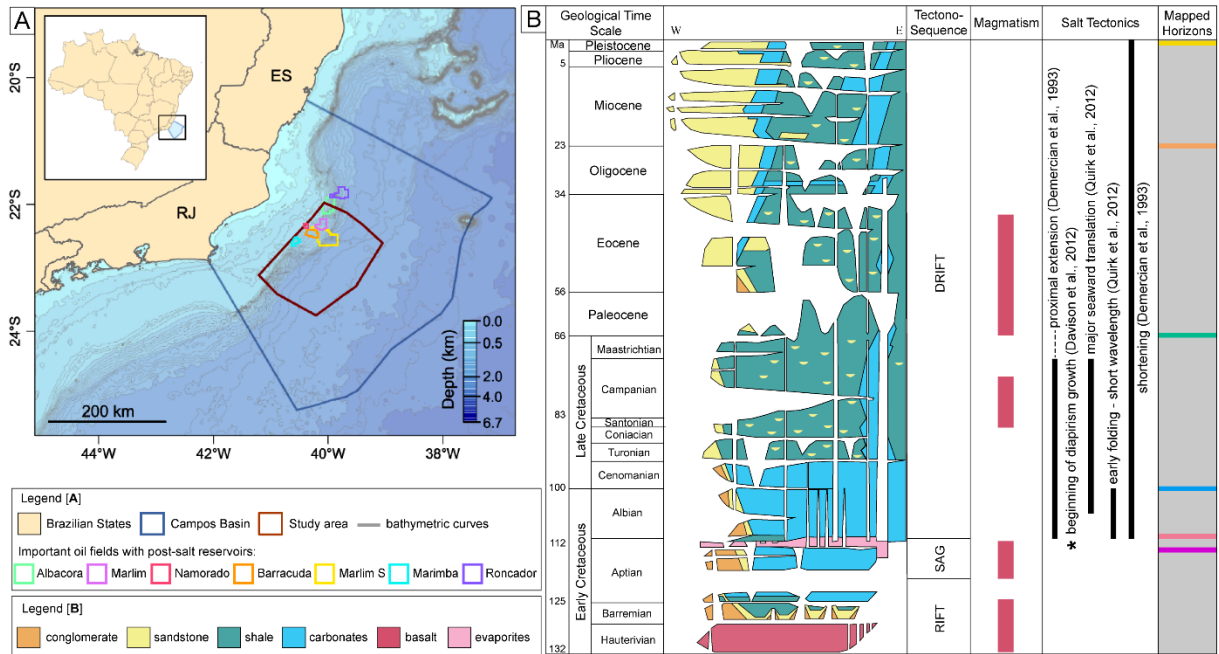


Figure 1. (A) Regional map showing the location of Campos Basin, the study area polygon and the main oil fields with post-salt reservoirs. (B) Simplified stratigraphic chart of Campos Basin (redrawn from Winter et al., 2007), with the main magmatic events and timing of the salt tectonics from previous publications; the last column shows the mapped horizons of this study with their designed colors.

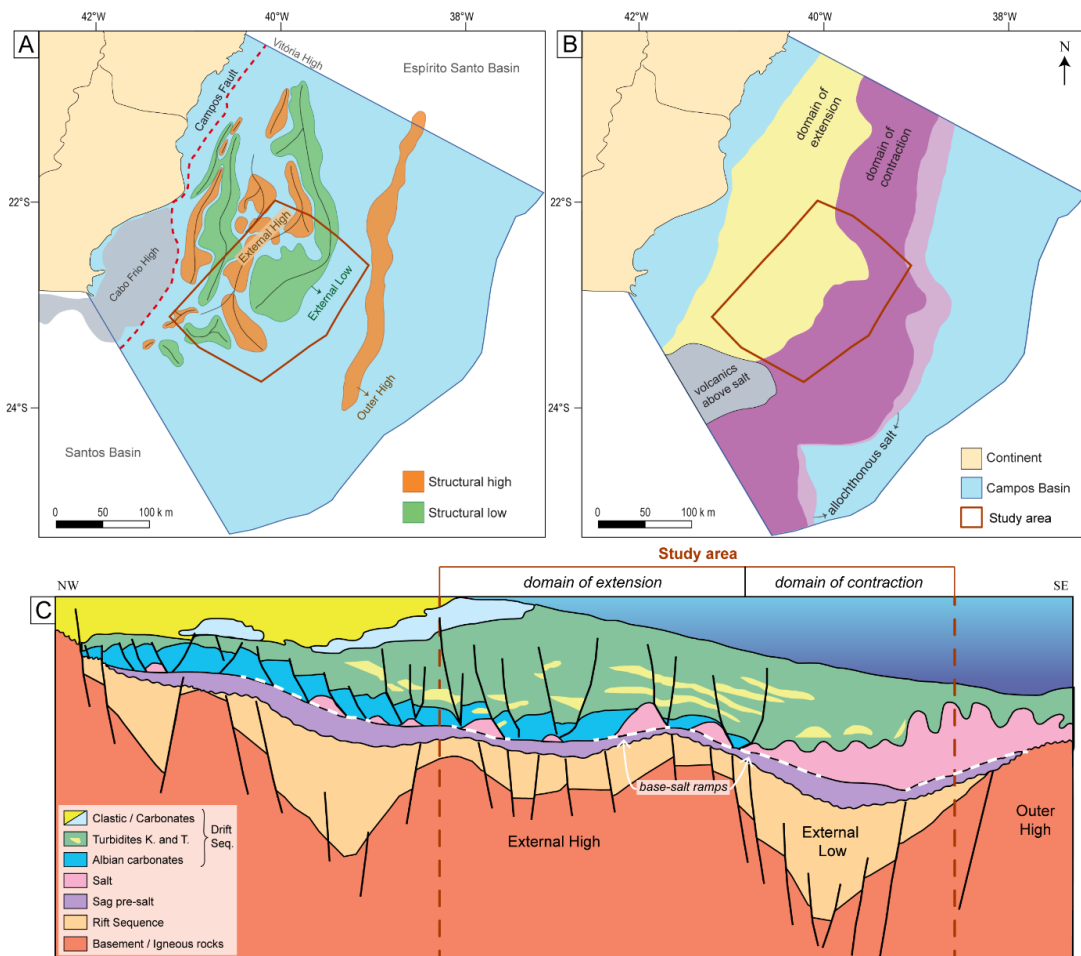


Figure 2. (A) Pre-salt structural framework of Campos Basin, redrawn from Guardado et al. (2000); Outer High and Cabo Frio High locations from Fetter (2009). (B) Salt-related structural provinces, modified from Davison et al. (2012); volcanics above salt location from Meisling et al. (2001). (C) Schematic cross section of Campos Basin, modified from Rangel et al., 1994.

3 - Database and Methodology

Our seismic reflection database comprises 146 2D lines and one 3D volume from the ANP (Brazil's National Oil, Natural Gas and Biofuels Agency) data library, covering an area of c. 23,500 km² of the central-southern platform of Campos Basin (Figures 1a and 3). Spacing between the 2D seismic lines ranges from around 1 to 30 km. The 3D volume covers c. 2,900 km², with inline (east-west) and crossline (north-south) spaced 12.50 m (Figure 3). The seismic surveys are time-migrated (PTSM Kirchhoff), zero-phase processed, with a display following SEG "normal" polarity; i.e. a downward increase in acoustic impedance is represented by a positive reflection event (i.e. white on displayed seismic profiles).

Within the study area there are 30 boreholes that contain well-logs (e.g. sonic travel time, bulk density, and gamma ray), and stratigraphic (i.e. age) and lithology data that help us constrain the age of the mapped horizons and the composition of the seismic-stratigraphic units they bound. The wells were tied to the seismic data through checkshot surveys. The interval velocity of the Aptian evaporites obtained from the well logs ranges from 4000 to 7000 m/s depending on the proportion of halite, anhydrite, and potash salts. Overburden strata are defined by interval velocities ranging from 1800 to 6000 m/s due to the highly varying densities of different lithologies (e.g. mudstone, sandstones, conglomerates, carbonates) with varying porosities.

We mapped four key horizons across the dataset additionally to the seabed: base of salt, top of salt, top Cretaceous and top Paleogene. Where possible, we mapped the top Albian (Figure 1b). We mapped the top Cretaceous and top Paleogene horizons because they represent regional seismic-stratigraphic unconformities that are easily identifiable throughout Campos Basin and which record major periods of salt-related deformation. The mapped surfaces display the present basin geometry; isochron (i.e. thickness) maps derived from these surfaces show the

distribution and evolution of salt-related sedimentary depocentres. All maps are presented in two-way travel time (TWT) milliseconds (ms) and have not been depth-converted (see below).

Evaporites are generally defined by significantly higher seismic velocities than encasing sedimentary rocks. In time-migrated seismic sections, thick salt structures may be underlain by velocity pull-ups in the base-salt surface and underlying, sub-salt reflections. Velocity pull-ups mimic the geometry of the overlying salt structures and may erroneously be interpreted as sub-salt structural highs (Marfurt and Alves, 2015). Such seismic artifacts occur in the SE portion of the study area where high-relief salt structures are present (Figure 4a); we therefore manually corrected our interpretation of the base-salt horizon to compensate for these pull-ups (Figure 4b). We then mapped the base-salt ramps, and calculated the dip-angle of these ramps in varying locations (Figure 4c) converting time (TWT, ms) to depth using a velocity of 4600 m/s – average interval velocity of the underlying rocks calculated from the well logs. Local base-salt dip angles were also calculated using the same methodology (Figure 4d).

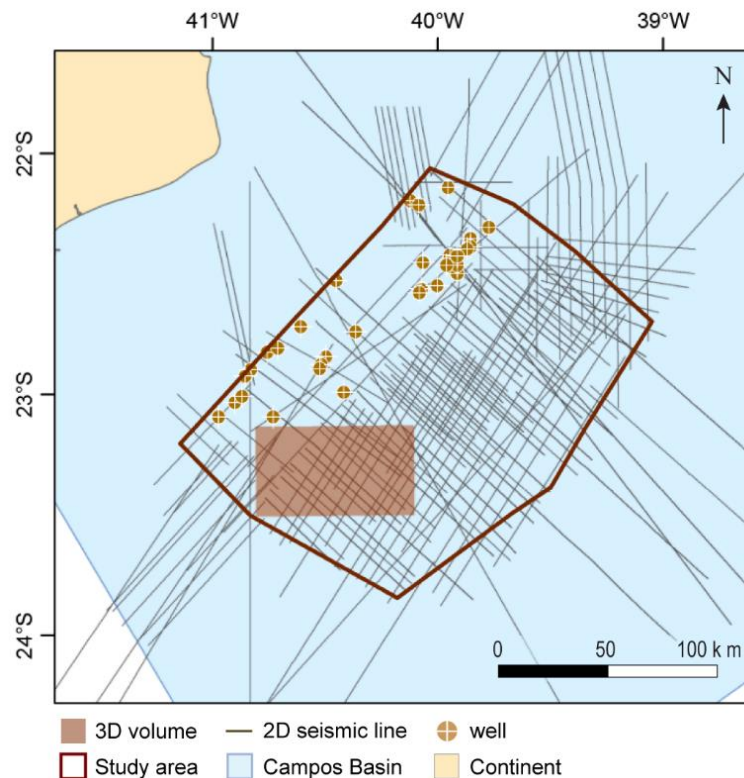


Figure 3. Dataset used in this study: 146 2D lines (or lines segments), one 3D volume and 30 boreholes.

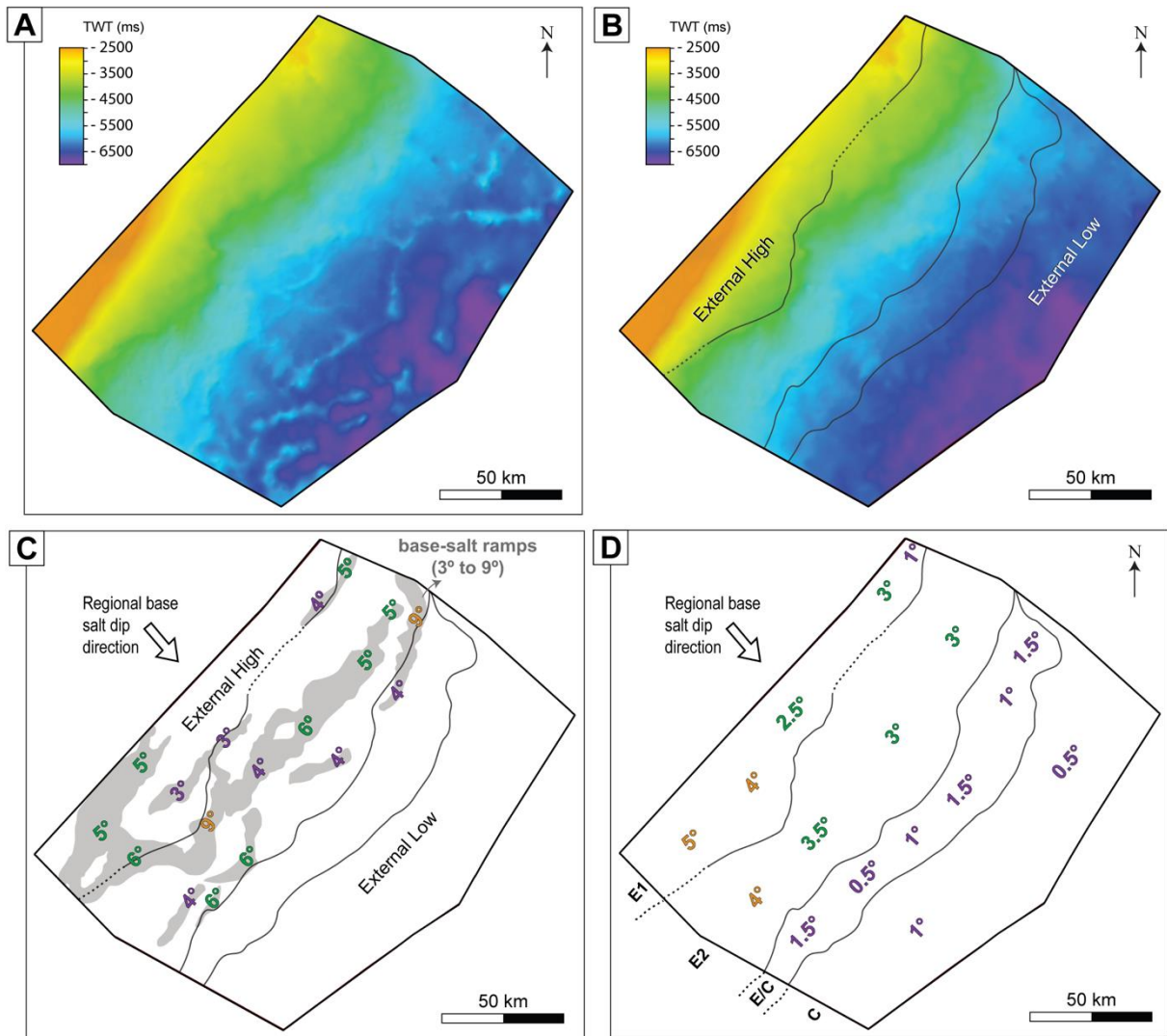


Figure 4. Time maps of the base-salt surface before (A) and after (B) the pull-up correction, showing doming dip to SE. (C) Mapped base-salt ramps shown in grey and their dip angles; the ramps are broadly subparallel to the margin, but with variable geometry along strike. The dip angles are plotted where they were calculated; they vary from 3° to 9°. (D) Average base-salt dip angles in different regions of each domain of deformation (shown in Figure 5).

4 - Base-salt structures

The base-salt surface dips regionally to the SE, with a mean dip of 2° (Figure 4a,b). Local changes in dip angle and direction define base-salt ramps (Figure 4c). In plan-view, elongate ramps trend NE, broadly subparallel to the margin, locally defining concave- or convex-seaward geometries. The main base-salt ramps define the boundary between the External High and the External Low (Figures 2 and 4b,c). These ramps have a maximum structural relief of c. 900 ms TWT, or c. 2 km (previous publications observe reliefs between 1.4 and 1.6 km – Dooley et al., 2017, figure 24; Davison et al., 2012, figure 6), and dip seaward

c. 3° to 9° (Figure 4c). Minor ramps within the External Low represent degraded fault scarps inherited from the earlier rift phase.

5 – Structural style of the salt and its overburden

The salt structures interpreted from the salt isochron map (Figure 5) present varying geometries and structural styles. Most structures trend broadly NE, sub-parallel to the underlying pre-salt rift-related ramps (Figure 5c). Exceptions to this occur in the SW of the study area, where salt-rollers trend N, and in the northeast, where a single E-trending salt wall is found. Salt structures are flanked by apparent primary salt welds (white areas in Figure 5a) or depleted salt; in these regions, sub-salt and supra-salt strata appear to be in direct contact.

Key overburden structures are displayed on the Top Salt to Top Cretaceous isochron map (Figure 6). These structures have broadly the same orientation as underlying salt structures (see detailed descriptions below) and where the underlying salt has pierced the entire Cretaceous succession, the latter is absent (white areas in Figure 6a,b). The types, dimensions and interpreted origins of the salt and overburden structures are summarized in Tables 1 and 2, respectively. We now present the distribution of these structures, which define the three main domains of thin-skinned, salt-detached deformation: extensional, contractional, and multiphase.

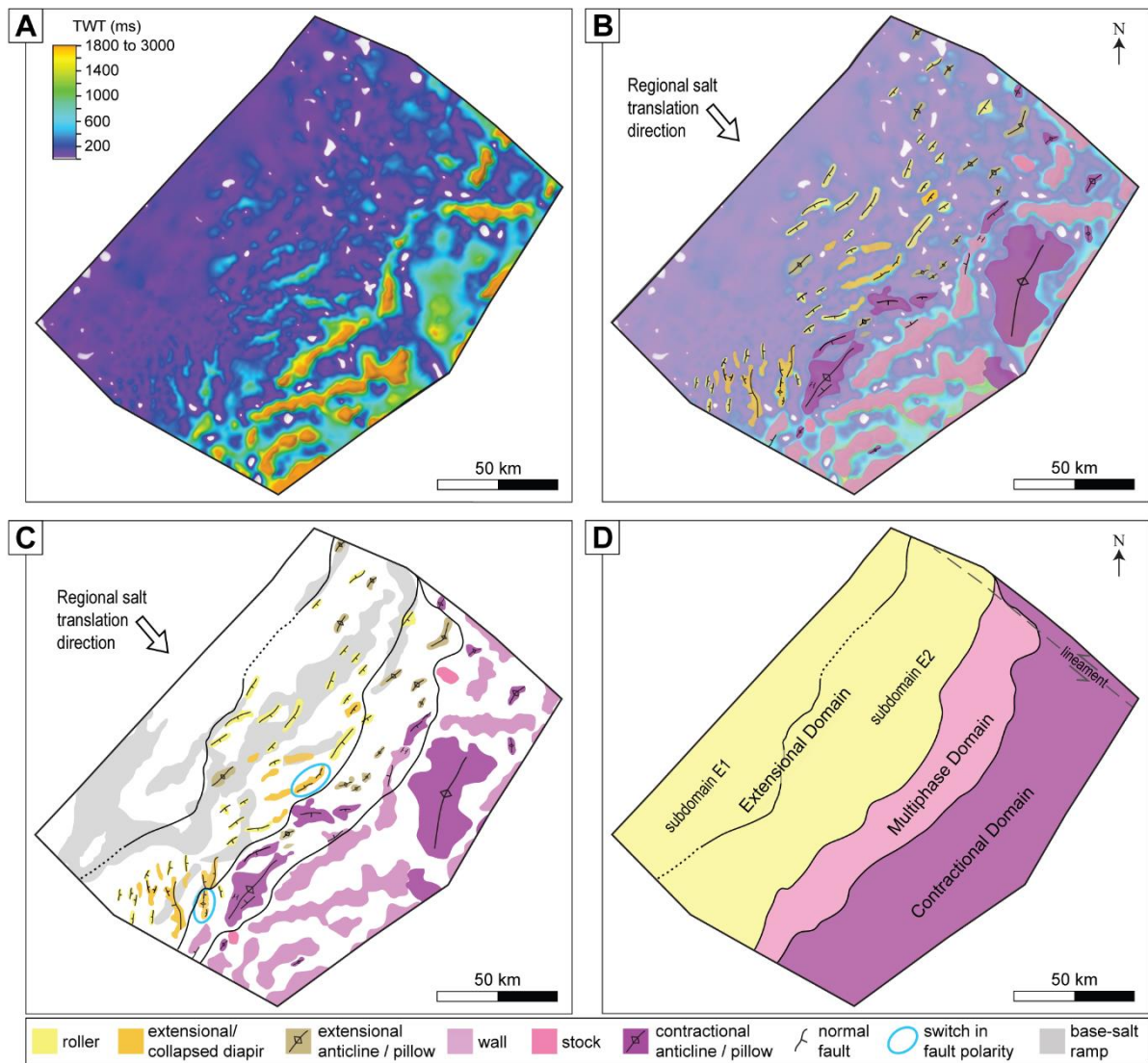


Figure 5. Salt isochron thickness map (A) with the interpreted salt structures in (B); areas of minimal thickness shown in white represent regions where salt is completely to incompletely welded. (C) Distribution of the salt structures across the study area, with the location of base-salt ramps in grey – colours of the structures within the multiphase domain follow their primary deformation. (D) Location of the domains of thin-skinned deformation; the boundary between E1 and E2 is partially dotted due to the scarcity of seismic lines in this region.

Table 1. Salt structures, their description, dimensions and genetic interpretation.

Structure	Example	Description (e.g. geometry, distribution, and overburden seismic-stratigraphy)	Dimension	Genetic Interpretation
Extensional salt rollers		<p>Relatively narrow, low-relief salt diapirs, bound on at least one side by a salt-detached normal fault (see Table 2). Strata in the footwall of this fault are up-turned and concordant with top salt; in the hanging wall, strata are in faulted contact with the salt. In upslope positions (Type 1 rollers; see column to right) they are relatively small, typically underlying and separating rafts (Table 2), and may be separated by primary welds; in downslope positions (Type 2 rollers; see column to right) they occur next to landward- or seaward-dipping salt-detached normal faults and associated extensional turtle structures (Table 2) or rollover systems. In toe-of-slope positions, salt rollers can also occur on top of salt anticlines.</p>	(1) 1–2 km wide; up to 200 ms TWT high.	<p>In upslope positions the seaward flow of salt drives overburden extension, which is accommodated by normal faulting. Differential loading of salt drives reactive diapirism and the formation of salt rollers that rise into the immediate hangingwall of salt-detached faults. In toe-of-slope positions, in the multiphase domain, later extension and faulting of salt contractional anticlines locally drove reactive rise and the formation of salt rollers.</p>
			(2) 4.7–20 km long; 1.5–5.5 km wide; up to 600 ms TWT high.	
Extensional/collapsed diapiric salt walls		<p>Triangular-shaped diapirs defined by wide bases and narrow crests. They are located in downslope positions, adjacent to Type 2 rollers. Diapirs are flanked and overlain by small, inward-dipping, salt-detached normal faults (Table 2). Flanking strata onlap or downlap onto, and often upturned against, top salt. Diapir crests are either rounded or U-/V-shaped; in the latter case, the shape arises due to the presence of horn-link cusps located in the hangingwall of overlying crestal faults (cf. salt rollers). The size and orientations of the faults vary, but they typically define crestal grabens filled with growth strata.</p>	5.3–12.3 km long; 1.4–5 km wide; up to 1300 ms TWT high.	<p>Thin-skinned extension of the overburden causes normal faulting and the formation of grabens and half-grabens. Differential loading of underlying salt drives reactive diapirism and salt wall formation. Continuing extension may cause diapirs to widen until the salt source layer becomes depleted and/or strongly restricted; diapir crests then begin to sag, driving normal faulting of and graben formation in overburden rocks.</p>
				Source: Vendeville and Jackson (1992a, b).
Salt anticlines and pillows		<p>Convex-up bodies of salt that have a concordant (i.e. non-diapiric) contacts with overburden strata. These structures occur across the entire study area; their dimensions increase towards the the downdip end. In downslope positions these structures are the core of extensional turtle structures (Table 2). Overburden commonly faulted (salt-detached normal faults - Table 2) and folded (extensional anticlines and contractional folds - Table 2).</p>	<p><i>extensional:</i> up to 15.8 km long up to 3.5 km wide up to 450 ms TWT high <i>contractional</i> 5.5–50.8 km long; 2.7–27 km wide; up to 1800 TWT ms high; $\lambda = 10\text{--}25$ km</p>	<p>Depending on their plan-view length-to-width ratio, these salt bodies are called pillows (ratio <2) or anticlines (ratio >2). In downslope they are associated to extensional turtle structures (Table 2), originated by thin-skinned extension (extensional salt anticlines and pillows). At the toe of slope and towards the downdip end of the study area, the structure form due to overburden shortening and salt inflation immediately seaward of base-salt ramps due to a salt flux imbalance associated with thickness variations of the salt layer (contractional salt anticlines and pillows).</p>
				Source: Dooley et al. (2017) and (2018); Jackson and Hudec (2017).
Diapiric salt walls and stocks		<p>Triangular to columnar salt structures in cross-section, characterised by discordant (i.e. diapiric) contacts with their overburden. In map-view these bodies are either sub-circular or elongated, located downdip the toe of slope. Often capped by an arched and faulted roof. High-relief structures underlie relief at the present seafloor. Commonly flanked by upturned megaflaps (sensu Rowan et al., 2016) of overburden strata which can be partially eroded by exposure (see example 2).</p>	<p><i>stocks:</i> up to 10 km long; up to 5.3 km wide; up to 1500 ms TWT high. <i>walls:</i> 14–72 km long; 2.2–14.4 km wide; up to 3000 ms TWT high.</p>	<p>Salt diapirs can grow via a range of mixed processes. Those in the contractional domain record mainly two mechanisms of diapiric rise: (a) passive diapirism, associated with syndepositional downbuilding of flanking diapirs); and (b) active diapirism, caused by regional thin-skinned compression, which also leads to overburden arching and faulting. Megaflaps may record a preceding stage of salt inflation and formation of a pillow or anticline, which was then broken through by a growing diapir.</p>
				Source: Rowan et al. (2016); Jackson and Hudec (2017).

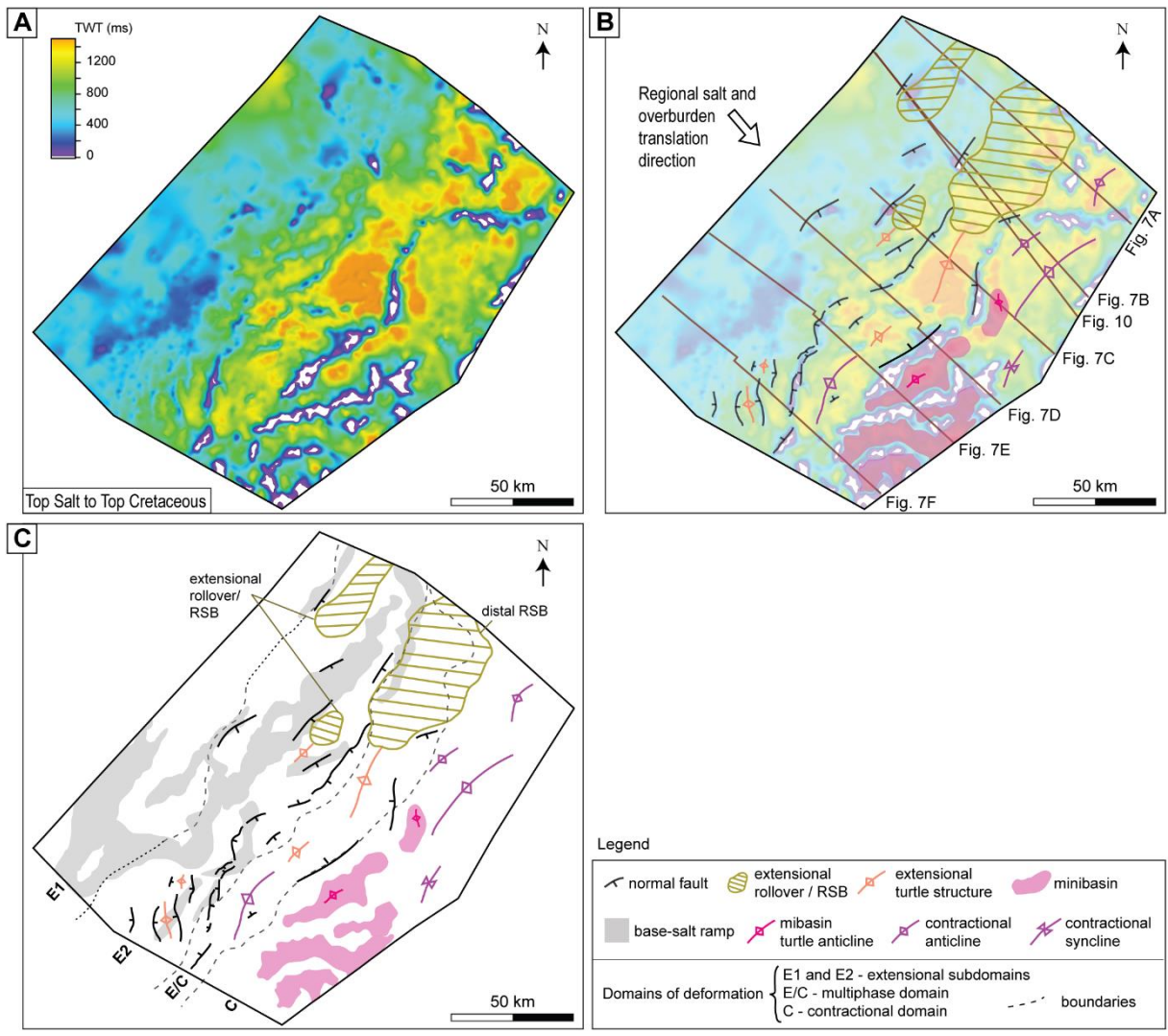
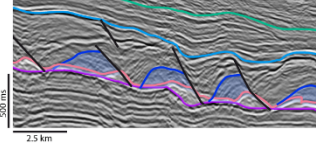
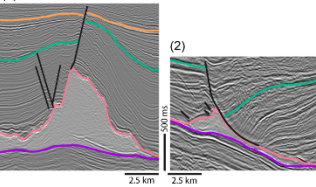
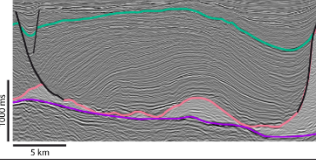
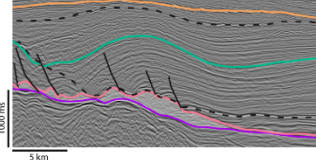
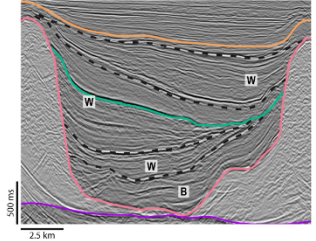
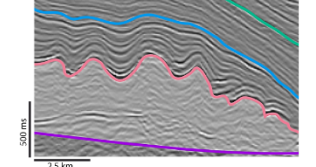


Figure 6. (A) Isochron thickness map from the Top Salt to the Top Cretaceous horizon. (B) Interpreted overburden structures related to salt tectonics onto the isochron thickness map of 6A; this map also shows the location of the seismic lines of figures 7 (and 8) and 10. (C) Distribution of the interpreted overburden structures in 6B, with base-salt ramps in gray and the domains of thin-skinned deformation.

Table 2. Salt-related overburden structures, their description, dimensions and genetic interpretation.

Structures	Example	Description	Dimension	Age of Growth Strata	Genetic Interpretation
Rafts		Rotated blocks (rafts) of overburden strata bound by salt-detached normal faults, separated by salt rollers and/or trough-like deposits of younger, synkinematic strata (see Table 1). Typically underlain by salt welds. Rafts occur updip in the study area.	2–3.2 km wide; 200–300 ms TWT high.	Early to mid-Albian.	Formed due to extensional dismemberment of overburden strata during gravity gliding. Synkinematic depocentres form between rafts. <small>Source: Quirk et al. (2012); Jackson and Hudec (2017).</small>
Salt-detached normal faults		Overburden-restricted normal faults that detach within salt. Bound salt rollers and associated rollover systems (example 2) and rafts, and can displace overburden strata capping the crests of salt anticlines (example 1) and as well as various types of diapirs (Table 1). May offset strata filling ramp-syncline basins. The faults dip landward- or seaward-, and are either listric or planar in cross-section.	up to 37 km long; up to 750 ms TWT of vertical throw.	<i>subdomain E1:</i> Albian; <i>subdomain E2:</i> Albian–mid-Neogene; <i>E/C Domain:</i> Albian–mid-Neogene; <i>Cont. Domain:</i> Albian–Recent.	Salt-detached normal faults accommodate thin-skinned extension of overburden. They can form: (i) in the proximal domains (ie. E1 and 2) due to the seaward flow of salt and associated overburden stretching; (ii) in the distal domain (i.e. C domain) due to outer-arc bending-related stretching of overburden above salt pillows and anticlines; (iii) due to overburden stretching above extensionally collapsing diapirs. <small>Source: Fort et al. (2004); Jackson and Hudec (2017).</small>
Extensional turtle structures		Anticlines bounded by oppositely and inward-dipping, salt-detached normal faults that also bound salt rollers and walls. Anticlines cored by salt pillows and anticlines (Table 1). Anticline-related growth strata are asymmetric, thickening towards one or both flanking faults. In map-view, these anticlines are elongated and trend parallel to their bounding normal faults.	up to 32.1 km long; up to 30 km wide; up to 1500 ms TWT high.	Albian–Early Paleogene.	Salt-detached normal faults with opposite dips are generated by thin-skinned extension. Salt flow into fault footwalls causing local overburden collapse, and ultimately the formation of a salt-cored anticline called a 'turtle'. <small>Source: Lundin (1992); Quirk et al. (2012).</small>
Ramp syncline basins		Synclinal basins located in the hanging-wall of salt-detached normal faults and associated rollover systems. Typically located above and slightly seaward of seaward-dipping base-salt ramps. RSB growth strata dip and thicken landward, defining a monoclinical geometry. Down-dip, the detachment surface (lower black dotted line) is marked by strata onlap or apparent downlap.	16–63.7 km long; 10–35 km of translation.	Albian–mid-Paleogene.	RSBs that form in response to the downdip translation of salt and its overburden across major base-salt ramps. The lateral distance between the top of the ramp and the seaward-most onlap (or apparent downlap) termination defines the magnitude of translation. <small>Source: Jackson and Hudec (2005); Jackson and Hudec (2017).</small>
Minibasins		Synclinal depocentres bounded by thick, diapiric salt. Depocentre strata thin towards and onlap onto bounding diapirs. Basal depocentre strata are symmetric, defining "bowl-shaped" geometries (B); these can be overlain by more asymmetric wedges of strata (W) thicken towards onto of the bounding diapirs. Basal megaflaps are common. Depocentres are floored by salt or a primary weld. Locally, multi-wavelength folds are developed within basal strata. In map-view, these depocentres are elongated parallel to bounding salt walls. Depocentres can be isolated or partially connected.	amplitude: 35–110 ms TWT and up to 1500 ms TWT $\lambda = 0.5\text{--}2.5$ km and 10–25 km	Albian–Top Paleogene.	Minibasins formed by density-driven subsidence of overburden into underlying salt. Subsidence may occur during lateral shortening. Bowl-shaped stratal packages (B) record symmetrical subsidence, whereas wedge-shaped packages (W) record asymmetric subsidence and minibasin tilting. Abrupt shifts in wedge depocentre location may reflect syn-subsidence shortening, which causes one bounding diapir to inflate more rapidly than the other. <small>Source: Jackson and Hudec (2017); Jackson et al. (2019).</small>
Contractional folds		Convex-up bodies, typically polyharmonic, with multiwavelength growth composed by early high-frequency folds and a larger wavelength growth. There can be faults dissecting the crest of the antiforms.	25–52.3 km long; 4.3–17 km wide; up to 1500 ms TWT deep.	Early Albian–Early Neogene.	High frequency folds formed when the overburden was thin, due to shortening immediately seaward of base-salt ramps in response to a salt flux imbalance associated with thickness variations of the salt layer. Subsequent regional thin-skinned compression promoted fold growth in larger wavelength. <small>Source: Cobbold and Szatmari, (1991); Fort et al. (2004)</small>

5.1. Extensional domain (E)

The extensional domain trends NW and corresponds to nearly half of the study area, with a minimum average width of c. 77 km (Figure 5). Based on the types of salt and overburden structures, we subdivided this domain into E1 (proximal) and E2 (distal) subdomains.

5.1.1. Description

Subdomain E1 defines the proximal, upslope portion of the extensional domain. In E1 the salt is broadly thin (0-300 ms, with an average of 80 ms) with limited top-salt relief and thickness variations (Figures 5, 6 and 7). Seismic profiles reveal small (200 to 300 ms high) salt rollers bounded by seaward-dipping, salt-detached normal faults (Table 1 and Figure 7d,e,f), and tilted raft-like blocks of Albian strata (Table 2). Where salt rollers are absent, salt is largely depleted (<50 ms) to (apparently) welded, or it forms small pillows (Figure 7a,b). The base-salt mean dip is 3° seaward, locally reaching 6° in NE-trending ramps (Figures 4c,d and 8).

Subdomain E2 occurs immediately downdip of E1. Salt thickness varies from 0-1450 ms, and numerous elongate, NE-to-N-trending structures are visible on the salt thickness map (Figure 5). The average base-salt dip is 3°, with NE-trending base-salt ramps dipping up to 9°, defining linear to locally concave- or convex-seaward geometries (Figures 4c,d and 8). The key salt and overburden structures in E2 are: (a) salt rollers and the associated salt-detached growth faults/rollover systems, which laterally transition to RSBs and extensional turtle structures; and (b) collapsed diapirs overlain by grabens and half-grabens (Tables 1 and 2).

In the NE portion of the study area, salt rollers and extensional rollovers dominate, and these can transition laterally to RSBs (Figure 6; Figure 7a,b); extensional anticlines or pillows occasionally underline RSBs (Figure 7a -structures 1; Figure 7b - structure 1). The central and southern regions of the study area are characterized by salt rollers bounded by seaward- or landward-dipping growth faults and flanking rollover systems (Figure 7c to f); which

occasionally define extensional turtle structures (Figure 7c - structure 2; Figure 7d - structure 2), or grabens above extensionally collapsed diapirs (Figure 7d - structure 3, Figure 7f - structures 1 and 2). There are also more complex extensional diapirs developed from salt rollers that appear to have grown with periodic switches in the polarity of the bounding faults (see *flip-flop salt walls* of Quirk et al., 2012; extensional diapir in Figure 9, inactive fault segments in white). Switches in fault polarity across extensional salt walls can be observed in the salt structure map (Figure 5c - blue ellipses). Salt rollers are dominantly located close to or above base-salt ramps (Figure 7d,e,f), whereas collapsed diapirs and grabens tend to overlie areas where the base-salt is flatter (Figure 7d,f). The extensional turtle structures are wider and longer in the central region in comparison to the north and south regions, where the growth faults are also longer (Figure 6b,c). The age of growth strata of the extensional turtle structures is from the Albian to the Top Cretaceous, cored by extensional salt anticlines/pillows (Figure 7d - structure 2; Figure 9) or anticlines/pillows of Albian strata (Figure 7c - structure 2). The age of growth strata of the salt-detached normal faults related to salt rollers and grabens onto collapsed diapirs are from the Albian to mid-Neogene (Table 2 and Figure 7).

5.1.2. Interpretation

The structures within the extensional domain vary along dip, defining the two previously described subdomains – E1 and E2 –, and they also vary along strike. To NE, salt in subdomain E1 is largely depleted to (apparently) welded or forms small pillows on a relatively flat-base-salt (Figure 7a,b). Subdomain E2 is characterized by salt rollers and extensional rollovers that can transition laterally to RSBs (Figure 7a,b), and the base-salt surface defines three main ramps (Figure 4c).

The formation of RSBs is conventionally defined as a product of translation of salt and its overburden across major base-salt ramps (Table 2) (Jackson and Hudec, 2005, 2017; Pichel et al., 2018). The RSBs in the extensional domain are associated to salt rollers and extensional

rollovers (Figure 7a - structure 1, 7b - structure 1; Figure 10), which means that translation of salt and its overburden downdip is partially accommodated by the displacement of salt-detached faults.

To SW of the study area, subdomain E1 is composed of a series of rollers associated to tilted blocks on wide base-salt ramps (Figures 7 and 8 d,e,f). In subdomain E2, from the centre to SW, there are salt rollers mostly associated to rollover extensional rollovers and turtle structures as well as collapsed diapirs with associated grabens (Figure 7c-f). Salt rollers typically occur onto base-salt ramps (Figures 7 and 8 c-f), whereas collapsed diapirs tend to develop further from the ramps, onto shallower basal slope angles (Figure 7 and 8 d,e,f).

According to Fort et al. (2004), zoning of the extensional structures occurs as a function of strain rate in the ductile salt layer. High ductile strain rate occurs at steeper slope angles, originating salt rollers in both subdomains: in E1 to the centre-SW of the study area, and in E2 in all regions of the study area. Contrarily, extensional (or collapsed) diapirs of the centre-SW E2 formed at shallower slope angles, where ductile strain rate is lower (see their figure 7). Subdomain E1 corresponds to the *sealed tilted blocks* subdomain of Fort et al. (2004), and E2 is the junction of the *growth fault and rollover systems* and *extensional diapirs* subdomains.

The overall base-salt dip angle of the extensional domain increases NE to SW (Figure 4d): even though the ramps maintain the same average dip, they become wider and/or more numerous (Figure 4c). Narrow and steep base-salt ramps likely favoured the formation salt rollers and extensional rollovers/RSBs in the northeastern portion of the study area (Figures 7 and 8 a,b,c). To the centre-SW, ramps wider morphology favoured the formation of rollover systems and extensional turtle structures associated to salt rollers (Figures 7 and 8 c-f).

5.2. Contractional domain (C)

5.2.1. Description

The contractional domain defines the downslope margin of the study area. This domain trends NE and has an average width of c. 39 km, being widest in the NE where it is up to 74.7 km wide to the north of a NW-trending, basement-involved lineament (Figure 5d). Base-salt is smoother in the contractional domain than in the extensional domain, with mean seaward dip varying from 0.5° to 1° (Figure 4d). Salt is thickest in this domain (up to 3000 ms) arranged in NE-to-E-trending broad salt anticlines underlying buckle folds, and salt walls and stocks (Table 1 and Figure 5) that are flanked by minibasins (Table 2 and Figure 6b,c).

One of the most prominent structure within the contractional domain is a large salt-detached fold belt (50.8 km long and up to 27 km wide; Figure 5), comprising stacked, multiwavelength folds, i.e., shorter-wavelength (0.5-2.5 km) and low-amplitude (35-110 ms) folds at top salt pass upwards into longer wavelength (10-25 km) and higher-amplitude (up to 650 ms) folds in the overburden (Figure 7b - structure 4; Figure 7c - structure 5). Similar structures are described by Davison et al. (1996), Demercian et al. (1993), Dooley et al. (2017) and Erdi and Jackson (2021).

Diapiric structures, commonly salt walls, predominate in the contractional domain (Figure 5c). These structures are up to 72 km long and 14 km high and triangular to columnar shaped in cross-section (Table 1). The diapirs are often capped by an arched or uplifted roof (Figure 7a - structure 3, 7b - structure 5, 7d - structure 7, 7e - structure 5, 7f - structure 3). Upturned megaflaps (*sensu* Rowan et al., 2016) frequently topped by erosional truncations flanking one side of the diapirs are common (Figure 7a - structure 3, 7e - structure 8, 7f - structures 3 to SE and 6) and can present early high-frequency buckle folds that are now rotated (Figure 7d - structure 7).

Post-salt Cretaceous overburden is thin to absent over salt walls in the contractional domain and very thick (up to 1800 ms) in the flanking synclinal depocentres (Figures 6 and 7d,e,f). When surrounded by upwelling salt, these synclinal depressions are referred to as *minibasins* (*sensu* Hudec et al., 2009) (Table 2). Minibasins occur centre to SW of the study area (Figure 6c); they can be overall symmetric (Figure 7e - structures 6) or asymmetric (Figure 7d – structure 6), floored by salt (Figure 7f - structures 4) or primary welds (Figure 7f - structure 5). Sometimes the minibasins can assume an antiformal, turtle-like shape (Figure 7c - structure 4).

5.2.2. Interpretation

Contractional structures in the study area consist of salt anticlines and pillows, and salt walls and stocks (Figure 5), presently located onto a smoother surface (mean dip of 0.75° - Figure 4d). The larger salt anticlines and a few salt walls present an early stage of high-frequency buckle folds (Figure 7b - structure 4, 7c - structure 5, 7d - structures 7 and 8). This type of folding forms by thin-skinned shortening when the overburden is thin (Cobbold and Szatmari, 1991; Fort et al., 2004), meaning contraction started soon after salt deposition, during the Lower Albian in Campos Basin (cf. Demercian et al., 1993; Quirk et al., 2012 - Figure 1c).

Early short-wavelength folds within polyharmonic folds form when the overburden is thin, either by local variations in salt flux across a basinward-dipping ramp (Dooley et al., 2017), or by regional shortening (Fort et al., 2004). After the formation of these early folds, the strength of the folded layer increases in response to synkinematic sedimentation, resulting in a progressive increase of fold wavelength (Cobbold and Szatmari, 1991; Fort et al., 2004). Shortening can become concentrated within anticlines and cause salt to be trapped and pinched in anticlinal cores, leading to the generation of contractional diapirs (see Figure 7d - structures 7 and 8) (Fort et al., 2004; Rowan et al., 2016 – see their figure 13). This mechanism of active rise of diapirs resulting in contractional outward-tilted megaflaps of the overburden and uplifted

and arched roofs by buckling (Table 2) (Jackson and Hudec, 2017), can evolve to passive diapirism once salt reaches the surface, and the structures grow downbuilding (Jackson and Hudec, 2017).

Not all diapiric structures in the study area have clear diagnostic features of thin-skinned shortening nor extension in their evolution, which means their growth history is dominantly caused by passive diapirism (e.g. Figure 7d - structure 7). However, these structures are considered to be part of the contractional domain given they were likely triggered by (or are associated with) shortening as they are associated with contractional structures.

Minibasins form primarily by due to subsidence of overburden into underlying salt. This subsidence is load-driven (i.e. overburden sinks and salt is expelled laterally), recorded as bowl-shaped, symmetrical packages, or wedge-shaped, asymmetrical packages (Table 2). Abrupt shifts in the wedges depocentres locations (Figure 7e - structure 6a; 7f - structure 5; Table 2) may reflect coeval lateral shortening, which causes one bounding diapir to inflate more rapidly than the other (Jackson et al., 2019). Turtle-like shaped anticlines within minibasins (Figure 7c - structure 4) originate due to partial or full depocentre inversion caused by minibasin welding at its centre, and the onset of subsidence and salt expulsion at its flanks (Trusheim, 1960; Peel, 2014).

5.3. *Multiphase domain (E/C)*

5.3.1. Description

This domain is located between the extensional and contractional domains, presently located at the toe of the External High to External Low ramps, and has a mean width of 25 km (Figure 5). Base-salt has average seaward dip varying from 0.5° to 1.5° (Figure 4d). Salt thickness in the multiphase domain ranges from 0-2100 ms, commonly composing NE-

trending, irregular to elongated structures, and more rarely, N- and E-trending structures (Figure 5).

To NE, this domain is fundamentally translational (or transitional), characterized by a large ramp syncline basin (RSB) (Figure 6c), which can be associated to salt rollers of subdomain E2 (Figure 7b - structure 2, 7c - structure 1; Figure 10). To the centre and south, the multiphase domain is characterized by three types of salt structures with a hybrid extensional-contractional evolution. The most common type consists of contractional anticlines that were subjected to later extension and normal faulting (Figure 7d - structure 4), which locally drove reactive rise and formation of salt rollers (Figure 9 - structure 2), and overlying grabens (Figure 7b - structure 3). The second most frequent type of structure comprises diapirs with passive and active growth history with landward-dipping normal faults that displace the diapir roof (Figure 7c - structure 3; Figure 7d - structure 5), and compose rollover systems which occasionally bound extensional turtle structures (Figure 7c - structure 3). Lastly, we observe an extensional diapir that was subsequently squeezed, with the latter phase of active diapirism driving arching and normal faulting of the diapir roof (Figure 9b - structure 1), or folding and uplift of strata above the collapsed diapir graben (Figures 9c and 7f - structure 2, between the Top Cretaceous and Top Paleogene).

5.3.2. Interpretation

Like the smaller RSBs (/extensional rollovers) in the extensional domain, the large RSB in the multiphase domain is partially bounded by salt-detached faults (Figure 7b - structure 2, 7c - structure 1; Figure 10). The balanced kinematic model in Figure 10 shows the hybrid origin of these structures (see also section 6).

The contractional anticlines that were subjected to later extension and normal faulting of the multiphase domain have two alternative origins. The first is that salt translated across two base-salt ramps, being deformed by the contractional hinge of the first ramp and

subsequently the extensional hinge of the second. The reconstruction of ramp syncline basins in the balanced kinematic model supports this origin (Figure 10). During the early Albian, salt flow across the updip base-salt ramp caused active salt upwelling across the contractional hinge at its base, folding the prekinematic strata (Figure 10g). Further translation across the downdip ramp reactivated the antiformal structure by extension generating two normal growth faults and reactive diapirism (Figure 10f). This multiphase deformation mechanism may be applied to the smaller structures of this domain (Figures 5c, 7b - structure 3, 7d - structure 4), which record deformation ceasing by the Top Cretaceous (Figure 10). Similar generation and deformation of salt structure across multiple base-salt steps is described in Kwanza Basin (Erdi and Jackson, 2021 – see their figure 9b), in Santos Basin (Pichel et al., 2019a) and from numerical models (Pichel et al., 2019b).

The second origin for the formation of contractional anticlines that were subjected to later extension and normal faulting is the seaward migration of extension through time, resulting in extensional inversion of previously contractional structures (Brun and Fort, 2011). Downdip migration of extension occurs after grounding of updip structures due to salt welding and/or margin progradation. This applies to the largest contractional structure to SW (Figures 5c, 9 - structure 2). This structure firstly grew into a multiwavelength salt anticline during the Albian and Late Cretaceous (see section 5.2.2), and later was extended, locally developing salt rollers as indicated by Paleogene normal fault growth strata (Figure 9 - structure 2). The salt was welded updip of the structure so that the system became pinned further updip whilst the inflated salt anticline was still able to flow and extend.

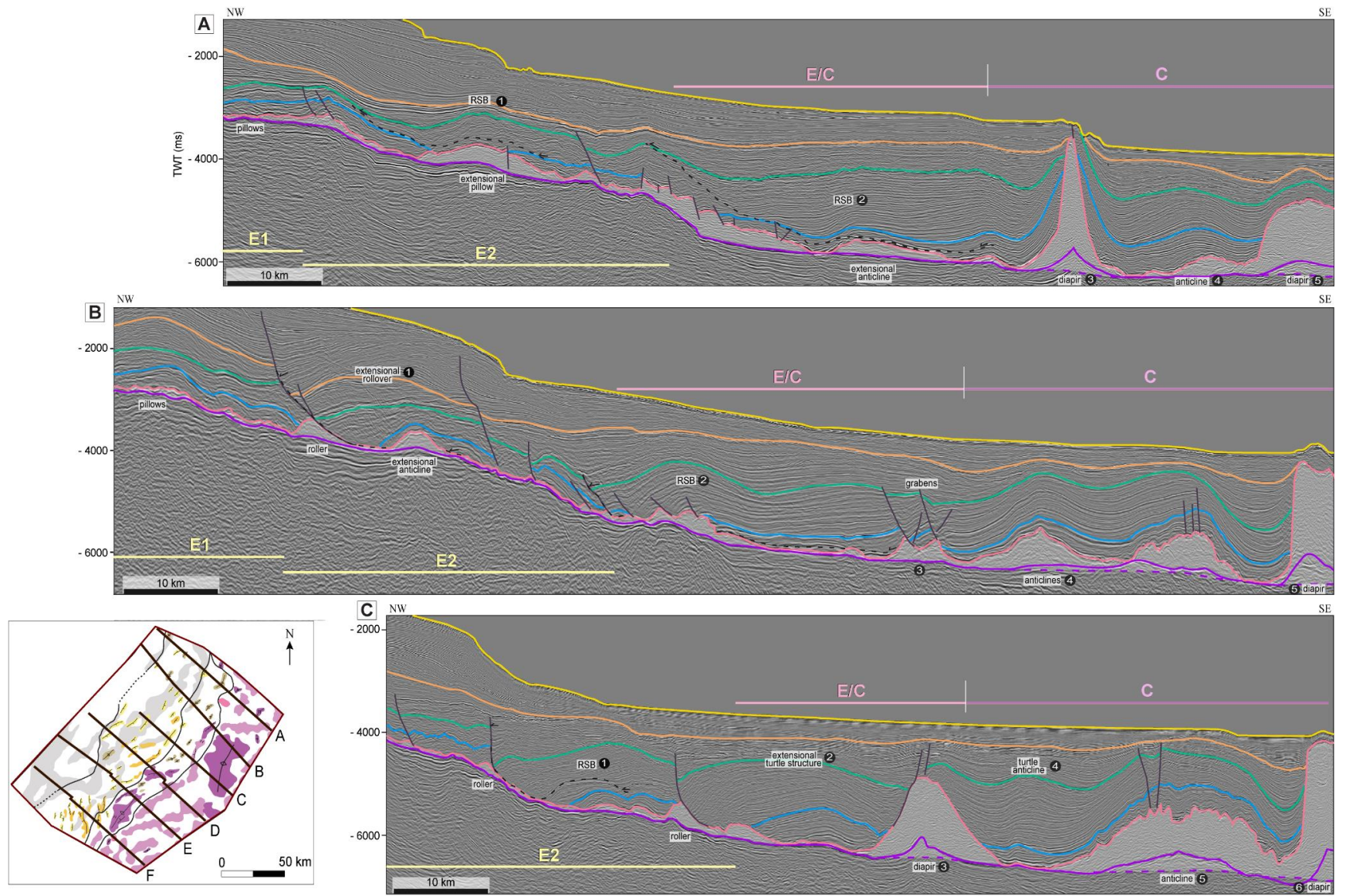
The mechanism of migration of extension related to salt welding also generated the diapirs that register compound active and passive growth with salt-detached normal faults (Figure 7c - structure 3, 7d - structure 5). Growth strata associated to the faults indicate that extension was active until the mid-Paleogene. Salt-detached normal faults accommodate thin-skinned extension originating sediment rollover, which can bound extensional turtle structures.

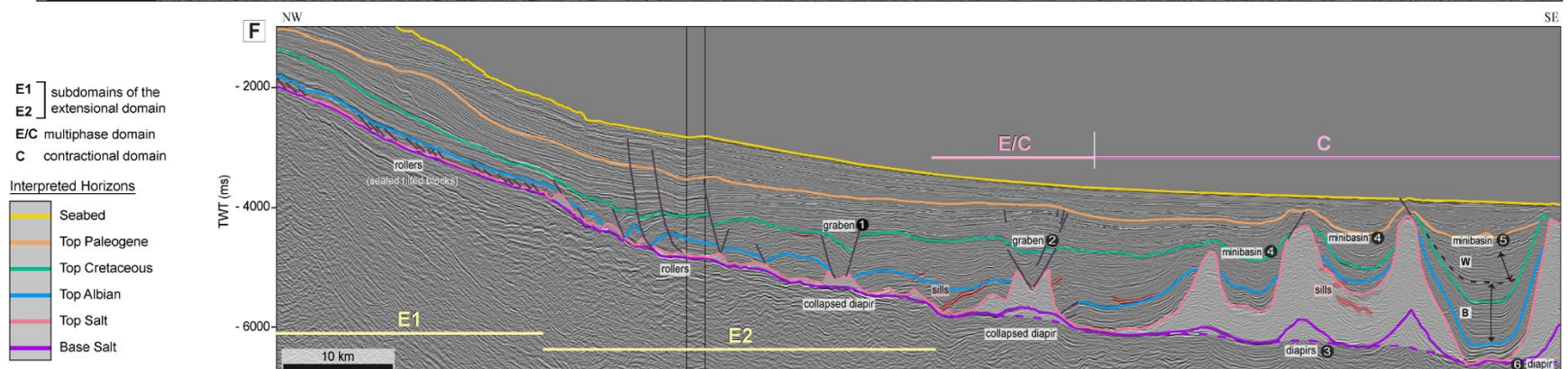
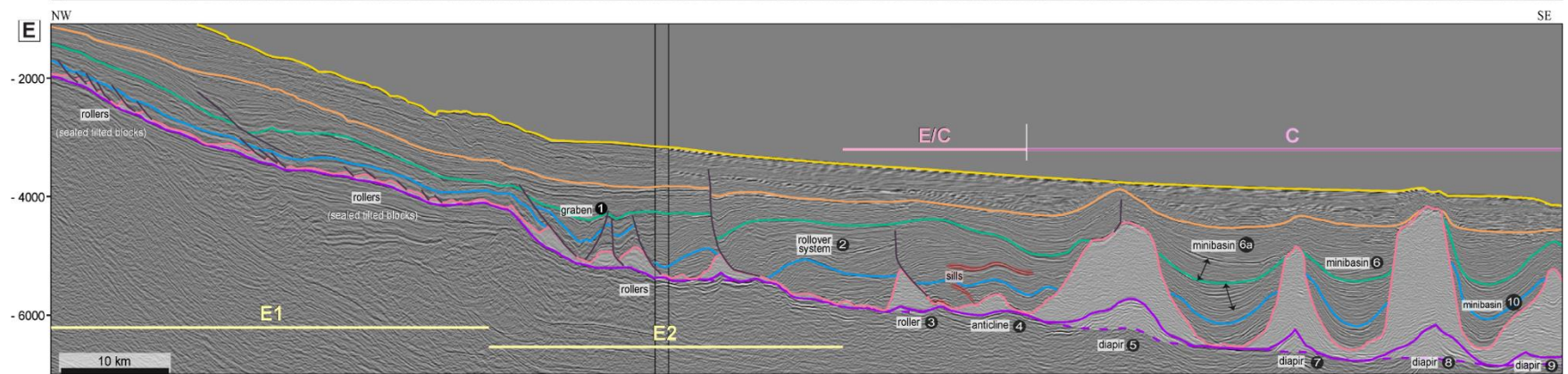
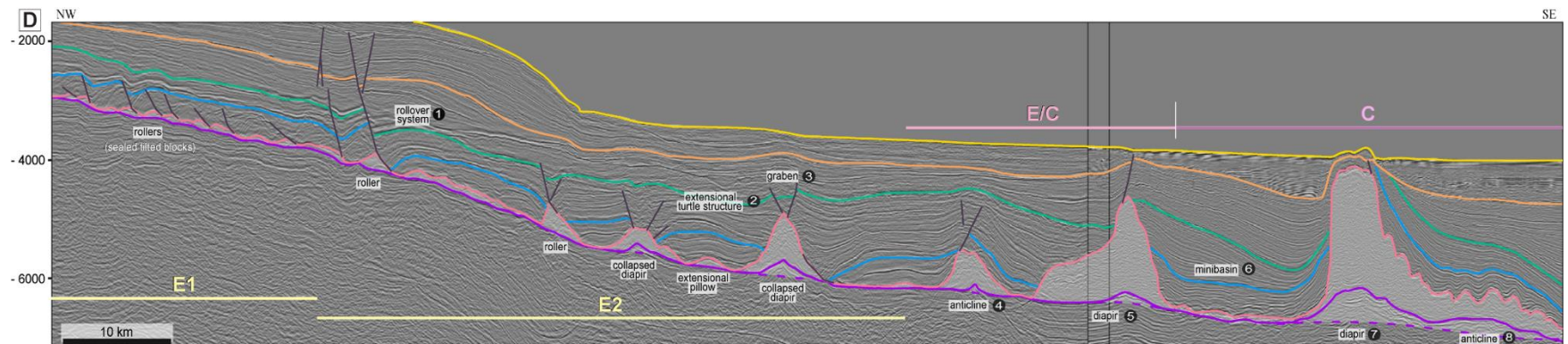
Lastly, in the multiphase domain there is one extensional diapir with later contractional deformation. This structure is located SW of the study area (Figure 9 - structure 1. Differential salt flow along base-salt steps may have caused the later contraction of the extensional diapir. The abundant presence of magmatic emplacements and intense faulting in the region may have also influenced the complex evolution history of this structure.

It is important to stress that the multiphase evolution of the aforementioned structures are heterogeneous, and may go unnoticed in an isolated 2D analysis (e.g. Figure 9 - structure 1).

(next two pages)

Figure 7. Interpreted dip lines in the north (A), (B), centre (C), (D), and south (E), (F) of the study area, with the interpreted seismic horizons, salt and overburden structures, and domains of deformation; the map left from (C) shows the locations of the lines onto the interpreted salt structures. Salt and overburden structures are numbered to facilitate indications in the text. Dotted lines on (A), (B) and (C) represent detachment surfaces of RSBs; dotted lines on (F) represents the shift from bowl-shaped minibasin to wedge-shaped; the arrows indicate minibasins depocentres. Seismic data supplied by ANP.





E1 } subdomains of the
 E2 } extensional domain
 E/C } multiphase domain
 C } contractional domain

Interpreted Horizons

Yellow line	Seabed
Orange line	Top Paleogene
Green line	Top Cretaceous
Blue line	Top Albian
Pink line	Top Salt
Purple line	Base Salt

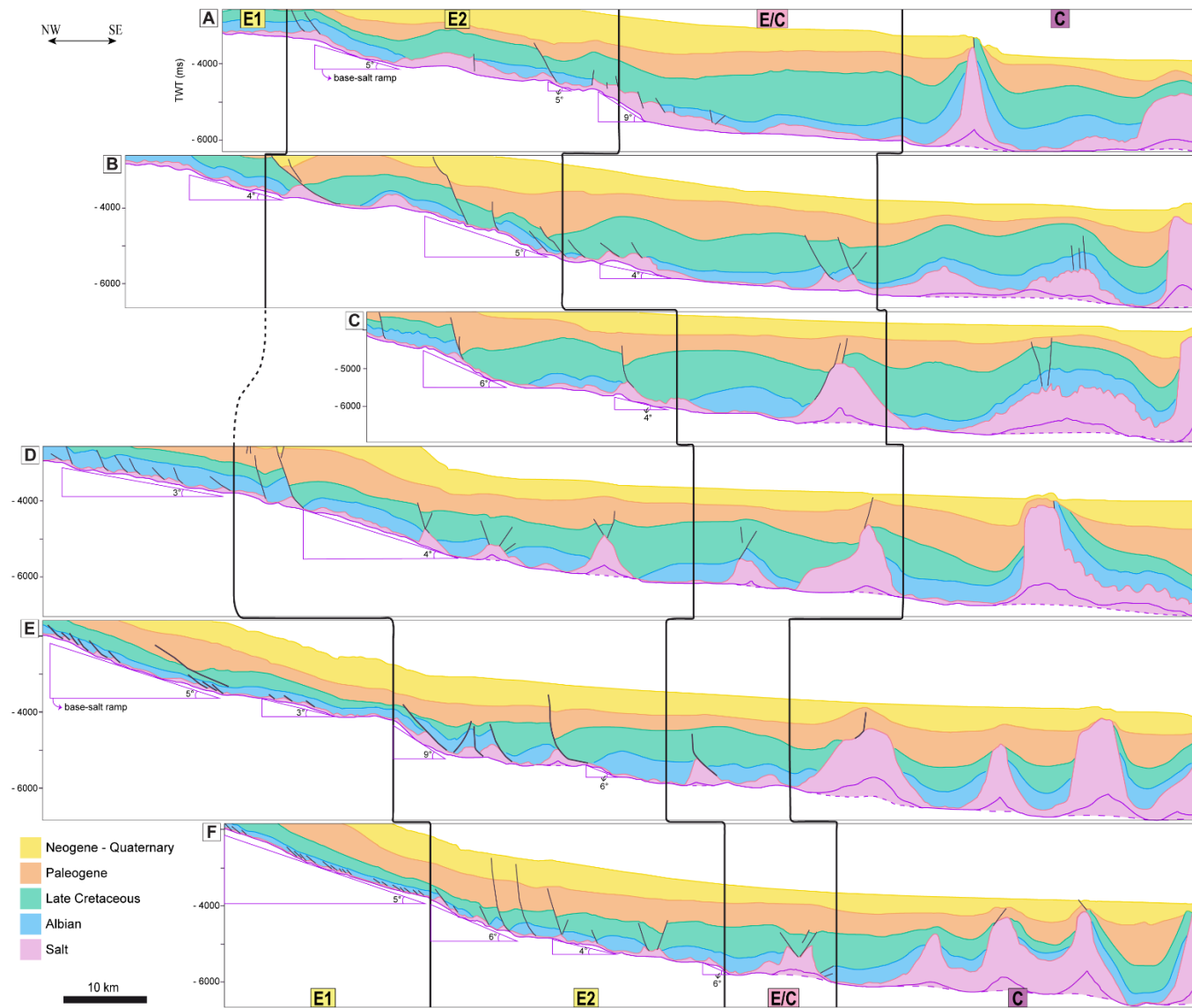


Figure 8. Stratigraphic intervals of the seismic geosections shown in Figure 7, with the spatial distribution of the deformation domains. The stratigraphic intervals have been coloured to highlight thickening and thinning relationships, indicating timing of the deformation. Base-salt ramps are indicated with triangles, together with their dip angles.

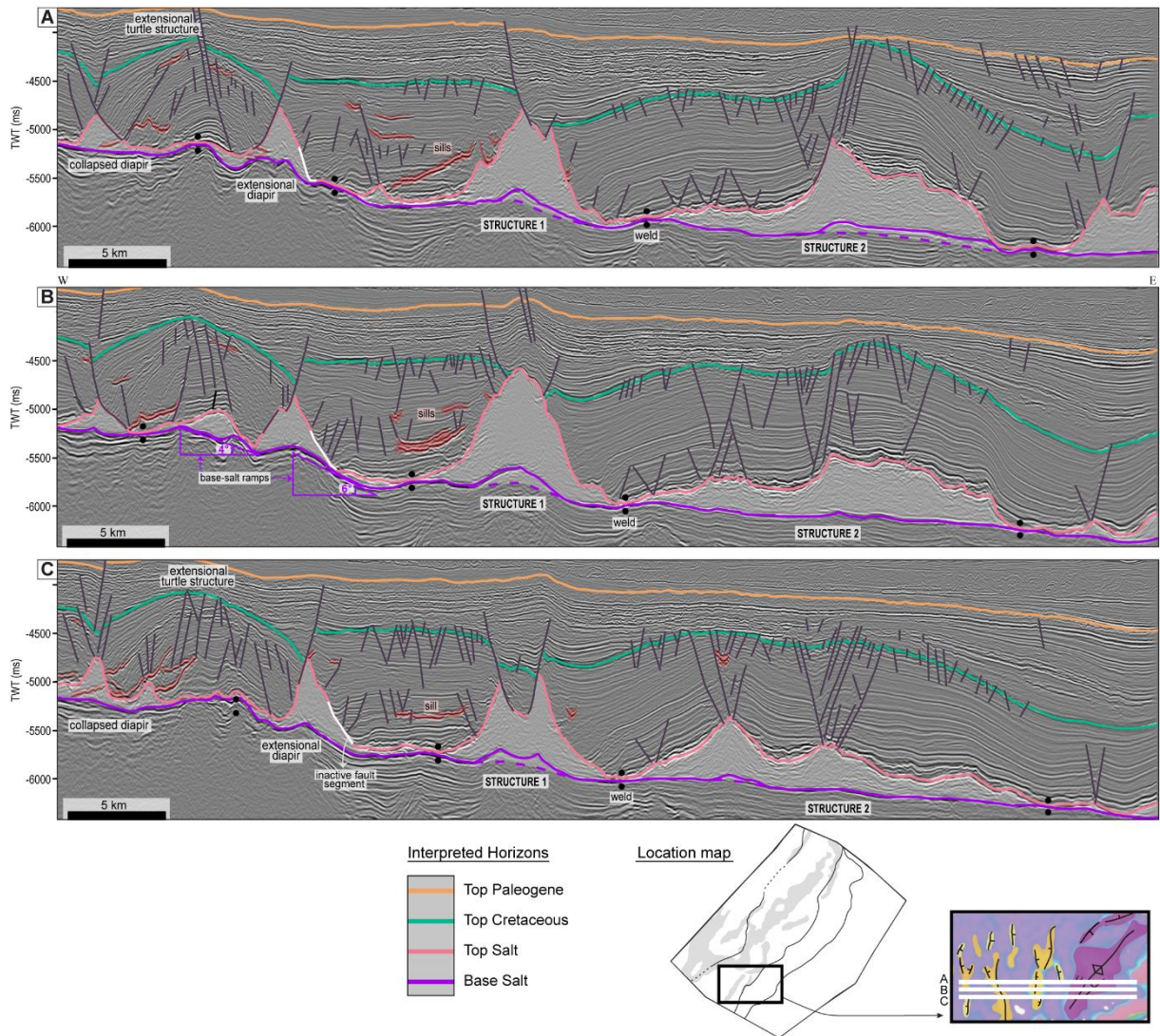
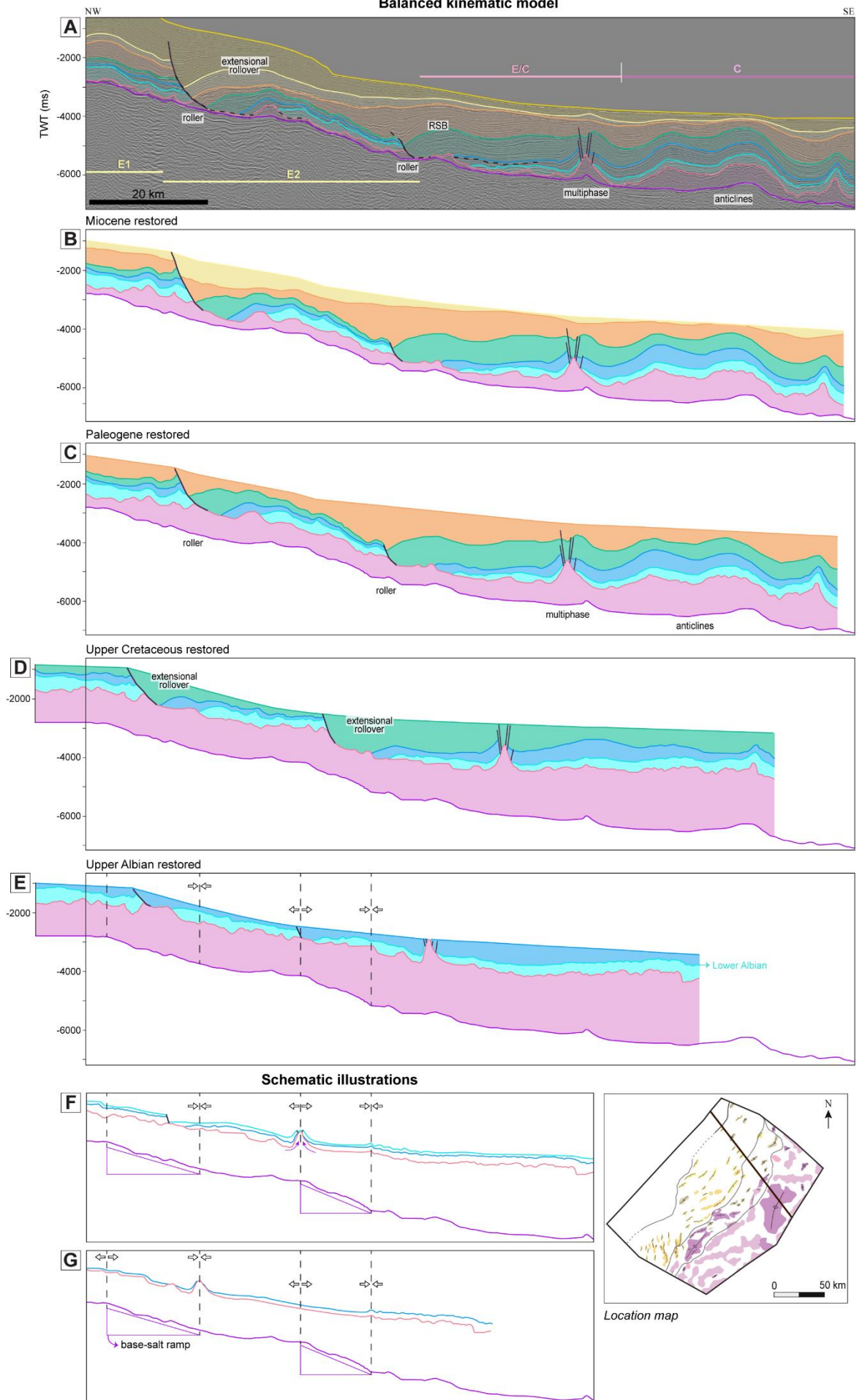


Figure 9. Interpreted seismic inlines of the 3D volume, with the interpreted seismic horizons, labelled salt and overburden structures, and base-salt ramps with their dip angles. (A) is north, (B) centre and (C) south – spacing between the lines is 1.6 km (see map in the bottom right for location). The sections show the boundary between the extensional domain (subdomain E2) and the multiphase domain, composed by structure 1 and structure 2. Note the abundance of sills and faults. Seismic data supplied by ANP.

Balanced kinematic model



(previous page)

Figure 10. (A) Interpreted seismic line 0239-0362 (see the map in the bottom right for location) used in the balanced kinematic model, shown in (B) to (E) – (B) is the restoration of the Miocene; (C) Paleogene; (D) Upper Cretaceous and (E) Upper Albian. See the methodology item for development details. (F) and (G) are schematic illustrations of salt deformation across base-salt ramps during the Albian. The colors of the horizons are indicated in Figures 2 and 7.

6 – Evolution of extensional and contractional deformation through time

Using temporal changes in sediment thickness patterns, seismic-stratigraphic relationships (i.e. onlap, erosional truncation), and balanced structural restorations, we reconstruct the evolution of the study area during three key time intervals: Albian to End-Cretaceous, Paleogene, and Neogene to Recent.

6.1. Albian to Top Cretaceous

During the Albian there were already thin-skinned extensional and contractional deformation ongoing as salt began to translate downdip towards the basin. Regional thin-skinned extension in the proximal subdomain E1 commenced and ceased during the Albian as shown by the occurrence of fault-bound Albian growth strata, with the fault tips sealed by post-Albian strata (Figures 7 and 8d to f). By the late Albian salt welds formed, associated with grounding of Albian rafts and the cessation of faulting (Fort et al., 2004).

In subdomain E2 extension continued later than in E1, reaching the end of the Cretaceous. Salt-detached normal faults and salt rollers formed to the centre and south of the study area, bounding extensional turtle structures of overburden strata (Figures 7c - structure 2, 8c and 9). Early reactive diapirs formed and subsequently collapsed, with most of this deformation ceasing by the end of the Cretaceous (Figures 7d-f and 8d-f).

To the north in E2 and in the multiphase domain, there was the development of extensional rollovers, as illustrated by the balanced kinematic model of line 0239-0362 in Figure 10a-e. The salt-detached normal faults bounding the salt rollers have formed during the Albian (Figure 10e). As salt translated downdip, the salt-detached faults continues to develop,

continually creating accommodation space, causing syn-kinematic strata to thicken towards the fault (Figure 10d).

Local contractional deformation induced by base-salt relief started in the early Albian, as recorded by growth strata within high-frequency buckle folds in anticlines in the contractional domain (Figures 7b - structure 4, 7c - structure 5, 7d - structures 7 and 8, 10f,g) and in the multiphase domain (Figures 9 - structure 2, 10f.g). With ongoing translation, early contractional structures that formed at the toe of seaward-dipping base-salt ramp undergone regional thin-skinned contraction and evolved into multiwavelength salt anticlines (Figures 7b - structure 4, 7c - structure 5, 7d - structure 8, 8 and 10), and one located in the multiphase domain (Figure 9 - structure 2). Some of these early contractional structures locally extended and faulted (Figures 7b - structure 3, 7d - structure 4, 10c-f) – with deformation of these multiphase structures ceasing near the end of the Cretaceous.

Regional thin-skinned contraction caused active diapirism in the end of the Cretaceous, as recorded by upturned megaflaps topped by erosional truncations (Figures 7a - structure 3, 7d - structure 7, 7f - structure 3 and 8a,d,f). Passive diapirism also occurred during the Cretaceous, recorded by stratal thickening within minibasins (e.g. Figure 7e - structure 6, 7f - structure 4). As extension migrated downdip, thin-skinned extension reached two salt walls which developed landward-dipping normal faults from the middle Cretaceous, bounding extensional turtle structures (Figures 5c, 7c - structure 2 and 8c).

6.2. *Paleogene*

Regional thin-skinned extension continued through the Paleogene. In subdomain E2, faulting associated with extensional turtle structures (Figures 7c - structure 2, 8c and 9).

In the multiphase domain, the RSB developed in response to further displacement of salt and its overburden, which caused strata to rotate downwards defining growth synclines with monoclonal geometries, typical of RSBs (Jackson and Hudec, 2005; Pichel et al., 2018) (Figure

10c,b). The multiwavelength anticline was subjected to extension and normal faulting as a consequence of welding further updip, which locally caused reactive rise and the formation of a salt roller (Figure 9 - structure 2). Faulted salt walls bounding extensional turtle structures within the multiphase domain have significant throw ceasing by mid-Paleogene (Figures 7c - structure 2 and 8c).

Regional thin-skinned contraction was also active throughout the Paleogene. The extensional diapir in the multiphase domain was compressed at this time, resulting in active rise and folding of the diapir roof (Figure 9 - structure 1). Salt-detached anticlines in the contractional domain amplified due to ongoing shortening and syn-kinematic sedimentation (Figures 7b – structure 4, 7c- structure 5, 8b,c and 10b,c). Diapirs in the contractional domain continued to grow actively and passively, with deepening of flanking minibasins until salt welding (Figures 7d -structure 6, 7f - structure 5 and 8d,f) and folding of diapirs roofs (Figure 7a - structure 5).

6.3. Neogene to Recent

The period between the Neogene to Recent records very little thin-skinned extension, with salt-detached normal largely being inactive by this time (Figures 7 and 8). The seaward flow of salt and overburden continued, at least in the extensional rollover/RSB (Figure 6c), until the middle Neogene (Figure 10a,b). Anticline growth in the contractional domain ceased in the Miocene (Figure 10a,b), whereas active rise of diapirs, presumably due to ongoing horizontal shortening, continued until recently and may still be ongoing (Figures 7a - structure 3, 7b - structure 5, 7c structure 6, 7d - structure 7 and 8a-d).

7 – Discussion

7.1. Base-salt relief as a control on salt tectonics

The major interpreted base-salt ramps in the study area delineate the boundary between the External High and the External Low (Figures 2 and 4). The ramps are overall linear, locally concave-convex (Figure 4c), with a maximum structural relief of c. 900 ms TWT (c. 2 km) and dip varying from 3° to 9°. The elongate ramps trend NE, perpendicular to the regional salt translation direction. Most salt and overburden structures trend NE, with exceptions to the southwest, seaward from the concave-convex ramps, where extensional structures are deflected to an N-trending orientation (Figure 5c). This is likely related to: (a) local changes in base-salt structure further updip and beyond our dataset, which redirected the salt flow to a bi-directional or radial gliding (Cobbold and Szatmari, 1991); and/or (b) the numerous volcanic sills in the region (Figures 7e,f and 9), which caused local changes in overburden strength.

Besides structures orientation, the base-salt geometry influences the types of salt and overburden structures, directly influencing the spatial variations within and between the domains of deformation. Regional extensional deformation was amplified as salt flowed across steeper surfaces (Figure 4d) – from the External High to the External Low and other interpreted base-salt ramps. Zoning of the structures (along dip and along strike) within the extensional domain occurs as a function of strain rate in the ductile salt layer: the steeper the slope angles the highest the ductile strain rate (Fort et al., 2004).

Seaward salt and overburden translation across base-salt ramps from the high block (External High) to the low block (External Low), and the associated flux and volume variations, resulted in local hinges of deformation. As the salt flows off a structural high onto a low, the salt flux decelerates as it encounters thick and slower-moving salt at the base of seaward-dipping ramps, ultimately generating local extensional hinges at the top of the ramps, and contractional hinges at the base (Dooley et al., 2017; 2018; Pichel et al., 2019a-b). This

mechanism is responsible for originating at least some of the contractional fold belts and anticlines in Campos Basin, and the subsequent extension of some of these structures. Dooley et al. (2017) interpreted a wide fold belt with polyharmonic folds in Campos Basin resembling the large antiform in Figures 7b,c and 10 (see their figure 24 for comparison)..

Structures in the high block, External High, become grounded by salt welding through time, and extension migrates downdip ultimately reaching the toe-of-slope. The migration of extension with time causes late regional extension of previously contractional structures and diapiric structures of the multiphase domain.

This study shows that although classic models of gravity gliding and spreading in salt-influenced passive margins are overall correct, they are an oversimplification and fail to explain the diversity of salt and overburden structures interpreted in Campos Basin. Even though the evaporites in the salt basins offshore SE Brazil were deposited during a period of relative tectonic quiescence, and the base-salt surface is overall quite smooth, there are few large-displacement faults (up to c. 2 km) that offset this surface. Downdip translation across these faults, i.e. base-salt ramps, locally alters deformation styles and salt tectonics kinematics.

7.1.2. Estimating the magnitude and rate of salt-detached translation

Seaward gravity-driven translation of salt and its overburden in Campos Basin started in the early Albian, lasting until at least the mid-Paleogene (Fig. 10). The distribution and evolution of key salt and overburden structures, and their relationship to base-salt relief, can indicate the magnitude of this translation.

Ramp-syncline basins (RSBs) have been used to determine the magnitude of salt-detached tectonic transport in passive margin basins, by measuring the distance between the top of the base-salt ramp and the (landward-directed) onlap point of the oldest intra-RSB strata

(Jackson and Hudec, 2005; Pichel et al., 2018). The RSBs in the Campos Basin are hybrid structures, evolving (in time) from and/or passing laterally (in space) into extensional rollovers due to temporal and spatial changes in salt thickness and ramp geometry (see item 5.1.2; Figure 10a-e). The hybrid extensional rollover-RSB in the NE (Figure 6c) started to form early in the Albian and was active until the mid-Neogene, recording a total overburden extension of c. 14 km (Fig. 10). The large RSB to SW distal RSB (Figure 6c) was active for a shorter period of time, containing Albian to mid-Paleogene growth strata, but records more post-Albian translation (c. 21 km). Thus, the total seaward translation of the overburden recorded by the RSBs is c. 35 km, comparable to that calculated by Dooley et al. (2017) elsewhere in the Campos Basin (see their figure 24).

An alternative way to estimate the magnitude of horizontal translation in salt basins is by measuring the distance between the most seaward end of a train of high-frequency buckle folds and the base of a seaward-dipping, base-salt ramp inferred to have generated them (Dooley et al., 2017). Applying this methodology to our dataset, where such buckle folds may plausibly have developed during the Albian (i.e., the major seaward-dipping base-salt ramp in the NW of the study area; see Figure 7b-d), we calculate translation magnitudes of c. 40 km (Figure 7b), c. 50 km (Figure 7c), and c. 60 km (Figure 7d) in the NE, centre, and SW of the study area, respectively.

The horizontal translation magnitudes estimated from the stratigraphic analysis of the RSBs (c. 35 km) differs significantly to those based on the present position of overburden buckle folds with respect to their inferred causal ramps (c. 40-60 km). We argue that RSBs provide a more certain record of the magnitude of horizontal translation in salt basins for the following reasons: (i) the translation magnitude calculated from RSB analysis is more consistent with the magnitude of salt-detached extension measured in the updip domain (Figs. 8 and 10); (ii) the salt nappe emplaced on oceanic crust at the seaward end of the Campos Basin, and which is at least partly the expression of the amount of horizontal translation updip (see

Jackson et al. 2015), is < 40 km wide (Figure 2b) (Davison et al. 2012), a value consistent with the magnitude of translation calculated from the RSBs; (iii) translation magnitudes calculated by RSB analysis in conjugate (i.e., Angolan; 13-23 km; Evans and Jackson, 2020; Erdi and Jackson, 2021) and neighbouring basins (i.e., Santos Basin; 28-32 km; Pichel et al., 2018) are more consistent with those defined here from comparable RSB analysis (c. 35 km); (iv) it is uncertain which ramp was responsible for the formation of the high-frequency buckle folds, i.e., was it the present toe-of-slope base-salt ramp or a more subtle ramp located further downdip?; (v) folding can occur due to regional overburden shortening and is not diagnostic of translation. Based on these observations, we infer that the Albian-aged high-frequency folds in the multiphase domain (Figure 9 - structure 2) did not form at the same base of the base-salt ramp associated with the formation of the RSBs, but may have instead formed at more subtle ramps located further downdip (Figures 4c and 5).

Having argued the *magnitude* of salt-detached translation in the Campos Basin is more likely c. 35 km than c. 40-60 km, we can now calculate the *duration* and *rate* of translation. Growth strata within the RSBs indicate translation started in the early Albian and lasted until the middle Paleogene, defining a duration of c. 65 Ma and a translation rate of c. 0.54 mm/year. Recent studies of RSBs in the conjugate Kwanza Basin, offshore Angola by Evans and Jackson (2019) and Erdi and Jackson (2021) demonstrate along-strike variability in both the magnitude and rate of Cenomanian-to-Recent salt-detached translation, i.e., from as little as 13 km at a rate of 0.13 mm/year in the NW of the study area, to 23.2 km at a rate of 0.23 mm/year in the SE. In the Santos Basin, offshore Brazil, Pichel et al. (2018) estimate a horizontal translation magnitude of 28-32 km, lasting for c. 50 Myr (i.e., from the end-Albian until the middle Paleocene) and defining a slightly faster translation rate than seen elsewhere (c. 0.7-0.8 mm/year). As argued by Pichel et al. (2018), Evans and Jackson (2019), and Erdi and Jackson (2021), this variability in the duration and rate of translation likely reflects changes in primary salt thickness and composition, the scale and distribution of base-salt relief, and local basement-

involved tectonic processes driving salt-detached deformation (i.e., margin uplift) (see also Dooley et al., 2017). Some combination of these controls may explain along-strike variation in RSB development and evolution in the Campos Basin. For example, base-salt surface is overall steeper in the SW compared to the NE (Figure 4d) and is defined by wider and more numerous base-salt ramps (Figure 4c). Davison et al. (2012) also suggest primary salt thickness increased south-westwards from c. 1.2 km to 2 km (see their figure 7), which is consistent with our observations, based on the RSB position, that the magnitude of translation was greatest in the SW.

7.2. Hydrocarbon exploration potential of Campos Basin

The Campos Basin is the second most prolific hydrocarbon basin in Brazil, being responsible for c. 33% of oil/gas production in Brazil (ANP real-time panel, 2021). The first oil discovery in the basin dates from 1970's, with the reservoir being Albian carbonates (Mohriak et al., 1990). Further exploration through the following decades led to the discovery of a further 41 oil and gas fields located 50-140 km off the Brazilian coast, under water depths of 80-2400 m. The fields are associated with a range of plays and have reservoirs in a variety of stratigraphic units (Bruhn et al., 2003).

Known petroleum systems of the Campos Basin are composed of Barremian/Aptian (i.e. sub- to intrasalt) and Albian (i.e. suprasalt) source rocks. Hydrocarbon migration from prerift source rocks to suprasalt reservoirs occurs through normal faults, across thin or welded salt (Guardado et al., 1989). The most important fields include reservoirs of post-salt turbidites in different stratigraphic levels, for example the Albacora (Miocene), Marlim (Oligocene to Miocene), Barracuda (Oligocene to Eocene) and Roncador (Maastrichian) fields (Figure 1A for fields location) (Bruhn et al., 2003; ANP report, 2015). Salt-related faults trap or strongly control most of the oil and gas accumulations in these turbidite reservoirs (Bruhn et al., 2003;

Mohriak et al., 2012). Subsalt reservoirs comprise rift (Barremian) and Aptian pre-salt carbonates (“coquines”) and clastics, and fractured syn-rift volcanics (Hauterivian) (Goldberg et al., 2017). The salt layer has a critical role for these deeper reservoirs, acting as an efficient seal rock.

The known post-salt reservoirs of the Campos Basin are mainly located within the thin-skinned extensional domain, which currently lies within relatively shallow water-depths (Figure 1A). This means significant unexplored areas may lie seaward of this location, in substantially deeper water. This study details the position and timing of salt-related deformation, key information required to push exploration barriers further basinward into the multiphase and contractional domains. We document multiwavelength salt anticlines in the multiphase domain; these could represent structural traps, with later extensional normal faults defining reservoir compartments (Figure 9 - structure 2). High-frequency buckle folds common in the contractional domain (e.g. Figure 7b - structure 4, 7c - structure 5) can also create structural traps (Jackson and Hudec, 2017) for hydrocarbons sourced from suprasalt, Albian source rocks. Megaflaps flanking diapirs in the contractional domain (e.g. Figure 7a - structure 3, 7e - structure 8, 7f - structures 3 to SE) can compose three-way truncation traps against salt; megaflaps can also act as a lateral seal for stratigraphic traps and have implications for fluid pressures in minibasins (Rowan et al., 2016). Diapirs could also be flanked by deep-water clastic reservoirs in pinch-out traps within minibasins (e.g. Figure 7d - minibasin 6 and adjacent diapirs 5 and 7, 7e – minibasins 6 and flanking diapirs 5, 7 and 8), similar to discoveries in the Gulf of Mexico (Booth et al., 2003). Finally, turtle anticlines within salt-withdrawal basins (e.g. Figure 7c - structure 4) can cause structural inversion of stratigraphic units and can create stratigraphic/structural traps, similar to those documented in east Texas, US (Wescott and Hood, 1994).

7 - Conclusions

We use 2D and 3D seismic reflection and borehole data from the south-central Campos Basin to characterise salt-tectonic structural styles and related evolution of salt and overburden structures. The key conclusions of our study are:

- Variations in dip angle and direction in the base-salt surface define base-salt ramps, which define the boundary between the External High and the External Low, basement structures originated by rift tectonics. The dip angle of the base-salt ramps vary from 3° to 9°, and the dip direction trend broadly to NE, in overall linear geometries and locally concave-convex. The maximum structural relief of the ramps is c. 900 ms TWT (or c. 2 km).
- The distribution of the interpreted salt and overburden structures define three domains of thin-skinned, salt-detached deformation: extensional – subdivided into subdomains E1 and E2 –, contractional, and multiphase.
- We interpreted three multiphase structures: (i) contractional anticlines that were subjected to later extension and normal faulting; (ii) diapirs with passive and active growth later subjected to regional extension, developing landward-dipping normal faults on the landward flank; and, lastly, (iii) an extensional diapir that was subsequently squeezed. The structures in the multiphase domain formed in response to multiple, kinematically-variable (extensional and contractional) phases of deformation over time and space.
- Base-salt relief caused local variations in salt flux, affecting the regional domains of deformation, controlling or influencing the types of generated salt and overburden structures, and their evolution through time and space.
- Ramp syncline basins record translation magnitude of c. 35 km, in a rate of c. 0.55 mm/year.

Acknowledgments

F.B.d. Amarante thanks CNPq (National Council for Scientific and Technological Development of Brazil) for the Sandwich Doctorate Abroad Scholarship (SWE). The authors gratefully acknowledge ANP (Brazil's National Oil, Natural Gas and Biofuels Agency) for providing the data and for the license to publish this article.

References

Amarante, F.B.d., Kuchle, J., Iacopini, D., Scherer, C.M.d.S., Alvarenga, R. dos S., Ene, P.L., Schilling, A.B., 2020. Seismic tectono-stratigraphic analysis of the Aptian pre-salt marginal system of Espírito Santo Basin, Brazil. *Journal of South American Earth Sciences* 98, 102474.

<https://doi.org/10.1016/j.jsames.2019.102474>

ANP (Brazilian Agency for Petroleum, Natural Gas and Biofuels). 2015. Geological Summary and Sectors on Offer. Retrieved from

http://rodadas.anp.gov.br/arquivos/Round_13/areas_oferecidas_r13/Sumarios_Geologicos/Sumario_Geologico_Bacia_Campos_R13.pdf

ANP Real-time Panel. 2021. Real-time web panel for production of oil and gas in Brazil.

Retrieved from <http://www.anp.gov.br/exploracao-e-producao-de-oleo-e-gas/paineis-dinamicos-de-producao-de-petroleo-e-gas-natural>

ANP (Brazilian Agency for Petroleum, Natural Gas and Biofuels), Exploration and Production Database Web Maps – BDEP (Banco de Dados de Exploração e Produção). 2020.

<http://www.anp.gov.br/exploracao-e-producao-de-oleo-e-gas/dados-tecnicos>

Booth, J.R., Dean, M.C., DuVernay, A.E., III, Styzen, M.J., 2003. Paleo-bathymetric controls on the stratigraphic architecture and reservoir development of confined fans in the Auger Basin:

- central Gulf of Mexico slope. *Marine and Petroleum Geology* 20, 563–586.
<https://doi.org/10.1016/j.marpetgeo.2003.03.008>
- Bruhn, C.H.L., Gomes, J.A.T., Del Lucchese, C., Jr., Johann, P.R.S., 2003. Campos Basin: Reservoir Characterization and Management - Historical Overview and Future Challenges, in: Offshore Technology Conference. Presented at the Offshore Technology Conference, Offshore Technology Conference. <https://doi.org/10.4043/15220-ms>
- Brun, J.-P., Fort, X., 2004. Compressional salt tectonics (Angolan margin). *Tectonophysics* 382, 129–150. <https://doi.org/10.1016/j.tecto.2003.11.014>
- Brun, J.-P., Fort, X., 2011. Salt tectonics at passive margins: Geology versus models. *Marine and Petroleum Geology* 28, 1123–1145. <https://doi.org/10.1016/j.marpetgeo.2011.03.004>
- Brun, J.-P., Mauduit, T.P.-O., 2009. Salt rollers: Structure and kinematics from analogue modelling. *Marine and Petroleum Geology* 26, 249–258.
<https://doi.org/10.1016/j.marpetgeo.2008.02.002>
- Chang, H.K., Kowsmann, R.O., Figueiredo, A.M.F., Bender, A., 1992. Tectonics and stratigraphy of the East Brazil rift system: an overview. *Tectonophysics* 213, 97–138.
- Cobbold, P.R., Szatmari, P., 1991. Radial gravitational gliding on passive margins. *Tectonophysics* 188, 249–289. [https://doi.org/10.1016/0040-1951\(91\)90459-6](https://doi.org/10.1016/0040-1951(91)90459-6)
- Contreras, J., Zühlke, R., Bowman, S., Bechstädt, T., 2010. Seismic stratigraphy and subsidence analysis of the southern Brazilian margin (Campos, Santos and Pelotas basins). *Mar. Petrol. Geol.* 27 (9), 1952–1980.

Davison, I., 2007. Geology and tectonics of the South Atlantic Brazilian salt basins. Geological Society, London, Special Publications 272, 345–359.

<https://doi.org/10.1144/gsl.sp.2007.272.01.18>

Davison, I., Alsop, I., Blundell, D., 1996. Salt tectonics: some aspects of deformation mechanics. Geological Society, London, Special Publications 100, 1–10.

<https://doi.org/10.1144/gsl.sp.1996.100.01.01>

Davison, I., Anderson, L., Nuttall, P., 2012. Salt deposition, loading and gravity drainage in the Campos and Santos salt basins. Geological Society, London, Special Publications 363, 159–

174. <https://doi.org/10.1144/sp363.8>

Demercian, S., Szatmari, P., Cobbold, P.R., 1993. Style and pattern of salt diapirs due to thinned gravitational gliding, Campos and Santos basins, offshore Brazil. Tectonophysics 228 (3–4), 393–433.

Dooley, T.P., Hudec, M.R., Carruthers, D., Jackson, M.P.A., Luo, G., 2017. The effects of base-salt relief on salt flow and suprasalt deformation patterns — Part 1: Flow across simple steps in the base of salt. Interpretation 5, SD1–SD23. <https://doi.org/10.1190/int-2016-0087.1>

Erdi, A., Jackson, C.A.L., 2021. What Controls Contraction in the Translation Domain of the Outer Kwanza Basin, Offshore Angola? Basin Research. <https://doi.org/10.1111/bre.12539>

Evans, S.L., Jackson, C.A.L., 2019. Base-salt relief controls salt-related deformation in the Outer Kwanza Basin, offshore Angola. Basin Research 32, 668–687.

<https://doi.org/10.1111/bre.12390>

Fetter, M., 2009. The role of basement tectonic reactivation on the structural evolution of Campos Basin, offshore Brazil: Evidence from 3D seismic analysis and section restoration. Marine and Petroleum Geology 26, 873–886. <https://doi.org/10.1016/j.marpetgeo.2008.06.005>

Fiduk, J.C., Rowan, M.G., 2012. Analysis of folding and deformation within layered evaporites in Blocks BM-S-8 & -9, Santos Basin, Brazil. Geological Society, London, Special Publications 363, 471–487. <https://doi.org/10.1144/sp363.22>

Fort, X., Brun, J.-P., Chauvel, F., 2004. Salt tectonics on the Angolan margin, synsedimentary deformation processes. Bulletin 88, 1523–1544. <https://doi.org/10.1306/06010403012>

Goldberg, K., Kuchle, J., Scherer, C.M.S., Alvarenga, R.S., Ene, P.L., Armelenti, G., De Ros, L.F., 2017. Re-Sedimented deposits in the rift section of the Campos Basin. Marine and Petroleum Geology 80, 412–431.

Guardado, L.R., Gamboa, L.A.P., Lucchesi, C.F., 1989. Petroleum geology of Campos Basin, Brazil: a model for producing Atlantic type basin. In: Edwards, J.D., Santagrossi, P.A. (Eds.), Divergent/Passive Margins Basins. AAPG Memoir 48, 3–36.

Guardado, L.R., Spadini, A.R., Brandão, J.S.L., Mello, M.R., 2000. Petroleum system of the Campos Basin, Brazil. In: Mello, M.R., Katz, B.J. (Eds.), Petroleum Systems of South Atlantic Margins. AAPG Memoir 73, 317–324.

Hudec, M.R., Jackson, M.P.A., Schultz-Ela, D.D., 2009. The paradox of minibasin subsidence into salt: Clues to the evolution of crustal basins. Geological Society of America Bulletin 121, 201–221. <https://doi.org/10.1130/B26275.1>

Jackson, C.A.-L., Duffy, O.B., Fernandez, N., Dooley, T.P., Hudec, M.R., Jackson, M.P.A., Burg, G., 2019. The stratigraphic record of minibasin subsidence, Precaspian Basin, Kazakhstan. Basin Research 32, 739–763. <https://doi.org/10.1111/bre.12393>

Jackson, C.A.-L., Jackson, M.P.A., Hudec, M.R., 2015. Understanding the kinematics of salt-bearing passive margins: A critical test of competing hypotheses for the origin of the Albian

- Gap, Santos Basin, offshore Brazil. *Geological Society of America Bulletin* 127, 1730–1751.
<https://doi.org/10.1130/b31290.1>
- Jackson, M.P.A., Hudec, M.R., 2005. Stratigraphic record of translation down ramps in a passive-margin salt detachment. *Journal of Structural Geology* 27, 889–911.
<https://doi.org/10.1016/j.jsg.2005.01.010>
- Jackson, M. P. A., Hudec, M. R., 2017. *Salt Tectonics: Principles and Practice*. Cambridge: Cambridge University Press. <https://doi.org/10.1017/9781139003988>
- Hudec, M.R., Norton, I.O., Jackson, M.P.A., Peel, F.J., 2013. Jurassic evolution of the Gulf of Mexico salt basin. *AAPG Bulletin* 97, 1683–1710. <https://doi.org/10.1306/04011312073>
- Kukla, P.A., Strozyk, F., Mohriak, W.U., 2018. South Atlantic salt basins – Witnesses of complex passive margin evolution. *Gondwana Research* 53, 41–57.
<https://doi.org/10.1016/j.gr.2017.03.012>
- Lundin, E.R., 1992. Thin-skinned extensional tectonics on a salt detachment, northern Kwanza Basin, Angola. *Marine and Petroleum Geology* 9, 405–411. [https://doi.org/10.1016/0264-8172\(92\)90051-f](https://doi.org/10.1016/0264-8172(92)90051-f)
- Marfurt, K.J., Alves, T.M., 2015. Pitfalls and limitations in seismic attribute interpretation of tectonic features. *Interpretation* 3, SB5–SB15. <https://doi.org/10.1190/int-2014-0122.1>
- Meisling, K.E., Cobbold, P.R., Mount, V.S., 2001. Segmentation of an obliquely rifted margin, Campos and Santos basins, southeastern Brazil. *AAPG Bulletin* 85 (11), 1903–1924.
- Mizusaki, A.M.P., Thomaz-Filho, A., Cesero, P., 1998. Ages of the magmatism and the opening of the South Atlantic Ocean. *Pesquisas* 25 (2), 47–57.

Mohriak, W.U., Mello, M.R., Karner, G.D., Dewey, J.F., Maxwell, J.R., 1989. Structural and stratigraphic evolution of the Campos Basin, offshore Brazil. In: Tankard, A.J., Balkwill, H.R. (Eds.), *Extensional Tectonics and Stratigraphy of the North Atlantic Margins*. AAPG Memoir 46, 577–598.

Mohriak, W.U., Mello, M.R., Dewey, J.F., Maxwell, J.R., 1990. Petroleum geology of the Campos Basin, offshore Brazil. Geological Society, London, Special Publications 50, 119–141. <https://doi.org/10.1144/gsl.sp.1990.050.01.07>

Mohriak, W., Nemčok, M., Enciso, G., 2008. South Atlantic divergent margin evolution: rift-border uplift and salt tectonics in the basins of SE Brazil. Geological Society, London, Special Publications 294, 365–398. <https://doi.org/10.1144/sp294.19>

Mohriak, W.U., Szatmari, P., Anjos, S., 2012. Salt: geology and tectonics of selected Brazilian basins in their global context. Geological Society, London, Special Publications 363, 131–158. <https://doi.org/10.1144/sp363.7>

Peel, F.J., 2014. How do salt withdrawal minibasins form? Insights from forward modelling, and implications for hydrocarbon migration. *Tectonophysics* 630, 222–235. <https://doi.org/10.1016/j.tecto.2014.05.027>

Pichel, L.M., Peel, F., Jackson, C.A.-L., Huuse, M., 2018. Geometry and kinematics of salt-detached ramp syncline basins. *Journal of Structural Geology* 115, 208–230. <https://doi.org/10.1016/j.jsg.2018.07.016>

Pichel, L.M., Jackson, C.A.L., Peel, F., Dooley, T.P., 2019a. Base-salt relief controls salt-tectonic structural style, São Paulo Plateau, Santos Basin, Brazil. *Basin Research* 32, 453–484. <https://doi.org/10.1111/bre.12375>

Pichel, L.M., Finch, E., Gawthorpe, R.L., 2019b. The Impact of Pre-Salt Rift Topography on Salt Tectonics: A Discrete-Element Modeling Approach. *Tectonics* 38, 1466–1488.

<https://doi.org/10.1029/2018tc005174>

Quirk, D.G., Hertle, M., Jeppesen, J.W., Raven, M., Mohriak, W.U., Kann, D.J., Nørgaard, M., Howe, M.J., Hsu, D., Coffey, B., Mendes, M.P., 2013. Rifting, subsidence and continental break-up above a mantle plume in the central South Atlantic. Geological Society, London, Special Publications 369, 185–214. <https://doi.org/10.1144/sp369.20>

Quirk, D.G., Schødt, N., Lassen, B., Ings, S.J., Hsu, D., Hirsch, K.K., Von Nicolai, C., 2012. Salt tectonics on passive margins: examples from Santos, Campos and Kwanza basins. Geological Society, London, Special Publications 363, 207–244. <https://doi.org/10.1144/sp363.10>

Rangel, H.D., Martins, F.A.L., Esteves, F.R., Feijó, F.J., 1994. Bacia de Campos. *Boletim de Geociências da Petrobras* 8 (1), 203–218.

Rowan, M.G., Peel, F.J., Vendeville B.C., 2004, Gravity-driven fold belts on passive margins. In McClay, K.K. (Eds.), *Thrust tectonics and hydrocarbon systems: AAPG Memoir 82*, 157–182.

Rowan, M.G., 2014. Passive-margin salt basins: hyperextension, evaporite deposition, and salt tectonics. *Basin Research* 26, 154–182. <https://doi.org/10.1111/bre.12043>

Rowan, M.G., Giles, K.A., Hearon IV, T.E., Fiduk, J.C., 2016. Megaflaps adjacent to salt diapirs. *Bulletin* 100, 1723–1747. <https://doi.org/10.1306/05241616009>

Szatmari, P., 2000. Habitat of petroleum along the South Atlantic margins. In: Mello, M.R., Katz, B.J. (Eds.), *Petroleum Systems of South Atlantic Margins: AAPG Memoir 73*, 69–75.

Trusheim, F., 1960. Mechanism of salt migration in northern Germany. AAPG Bulletin 44, 1519–1540.

Vendeville, B.C., Jackson, M.P.A., 1992 a. The rise of diapirs during thin-skinned extension. Marine and Petroleum Geology 9, 331–354. [https://doi.org/10.1016/0264-8172\(92\)90047-j](https://doi.org/10.1016/0264-8172(92)90047-j)

Vendeville, B.C., Jackson, M.P.A., 1992 b. The fall of diapirs during thin-skinned extension. Marine and Petroleum Geology 9, 354–371. [https://doi.org/10.1016/0264-8172\(92\)90048-j](https://doi.org/10.1016/0264-8172(92)90048-j)

Wescott, W.A., Hood, W.C., 1994. Hydrocarbon Generation and Migration Routes in the East Texas Basin. Bulletin 78. <https://doi.org/10.1306/bdff908c-1718-11d7-8645000102c1865d>

Winter, W.R., Jahnert, R.J., França, A.B., 2007. Bacia de Campos. Boletim de Geociências da Petrobras 15(2), 511–529.